Order and disorder in neurofilament proteins

A thesis submitted in partial fulfillment
of the requirements for the degree
of
Doctor of Philosophy

by

Micha Kornreich

Under the supervision of
Prof. Roy Beck

Presented to the senate of the Tel Aviv University

November 2016

This work was done under the supervision of Prof. Roy Beck

Abstract

It has long been assumed that protein function arises from its unique 3D structure, which determines the specific protein functionality. However, in the past two decades it was found that approximately 50% of human proteins are intrinsically disordered proteins (IDPs), *i.e.* proteins that contain long structurally disordered regions. These regions were subsequently shown to be critical for the designated functions of IDPs [1, 2]. As the conformation of these regions under physiological conditions resembles that of a random walk polymer, their investigation naturally calls for experimental and theoretical tools taken from polymer physics and statistical mechanics.

This poses IDPs at the interface between biology and physics. As physicists, the complexity and diversity of IDPs provide new experimental opportunities to tackle open questions in polymer science. At the same time, the application of physical analysis to IDPs offers novel insights on their biological functionality.

In this thesis I experimentally investigate the compression response and liquid crystalline behavior of complex bio-polymers, including neurofilament (NF) proteins and artificial DNA-protein bottlebrushes. Together with our colleagues, we use small-angle X-ray and dynamic light scatterings as well as optical, electron and force microscopies to measure polymeric structures and interactions. Our analysis follows a polymer physics approach, aimed at unraveling the underlying molecular mechanisms that govern IDPs organization.

The compression response of NF hydrogel networks are measured at various environmental conditions. NF proteins are IDPs that form 10 nm wide elongated bottlebrushes, which condense into an hydrogel at high concentrations. One of their main roles is to mechanically support cells, which is achieved by interactions between protruding disordered protein regions. Under near-physiological conditions, we show that the steric and electrostatic repulsive forces that dominate the NF stress response are comparable. Accordingly, we demonstrate how the IDPs' compression response can be efficiently controlled by biological manipulation of their electrostatic charges. As the compression increases, the

largely negatively-charged NF disordered regions can be well-approximated by uniformly charged ones. The flexible regions allow for the stress-responsive NF hydrogel to compress 20-fold without yielding, which may explain why IDPs are essential components of the supportive skeletons of cells.

The polyampholytic nature (*i.e.*, having both negative and positive charges) of the NF disordered regions is manifested only at low to moderate compression, as we experimentally reveal using a set of genetic and enzymatic modifications. There, we find that electrostatic cross-bridges between oppositely charged protein segments dominate the hydrogels' size and anisotropic organization. Such relation between cross-bridging and anisotropy was rarely considered before, and may explain why NF form liquid crystals, which is atypical for bottlebrush molecules.

The ability to manipulate the spacing, orientation and mechanical response of NF hydrogels using few modifications of their disordered regions, demonstrates the critical role played by IDP sequence. This signifies that protein disorder must not be confused with randomness. In fact, the physical analysis shows how sequence specificity, and particularly charge, do matter.

Table of Contents

Acknowledgments **iii**

Publications **v**

1: Introduction **1**

1.1 Polymer brushes 4

1.2 Intrinsically disordered proteins 7

1.3 The cytoskeleton 8

1.4 Intrinsically disordered neurofilament proteins 8

1.4.1 Biological roles of neurofilament proteins 11

1.5 Bottlebrush and liquid crystals 13

1.6 Methods for soft matter characterization 15

1.6.1 Small angle X-ray scattering 15

1.6.2 Cross-polarized microscopy 16

1.6.3 Atomic force and electron microscopy 18

1.6.4 Protein expression and purification 18

2: Main thesis papers **21**

2.1 Composite bottlebrush mechanics: α-Internexin fine-tunes neurofilament network properties 22

2.2 Order and disorder in intermediate filament proteins 23

2.3 Neurofilaments function as shock absorbers: compression response arising from disordered proteins 24

2.4 Phosphorylation-induced mechanical regulation of intrinsically disordered neurofilament protein assemblies 26
2.5 Liquid crystals of self-assembled DNA bottlebrushes 27
2.6 Loss of bottlebrush stiffness due to free polymers 28
2.7 Cross polarization compatible dialysis chip 29

3: Additional papers 30

3.1 Peptide self-assembly as a strategy for mimicking a bacterial pilus nanofiber 30
3.2 Neurofilament assembly and function during neuronal development . . . 31
3.3 Modern X-Ray scattering studies of complex biological systems 32

4: Discussion 34

References 48

Appendix A: Appendix: protocols 60

A.1 Native protein purification protocol 60
A.2 Recombinant protein purification and expression 60
A.3 Negative staining of neurofialments for transmission electron microscopy 60
A.4 Sample preparation for atomic force microscopy 60
A.5 Protein concentration determination by mini-Bradford assay 60
A.6 Neurofilament self-assembly protocol 60

Acknowledgments

I would like to thank the many persons which were involved in this PhD work. First, to Eti, the ultimate working partner, whose many complementary interests and skills made our teamwork together ideal. Your hard work and resilience saved us (and our synchrotron runs) so many times in the course of our joint work. I would also like to thank Rona Shaharabani, Ram Avinery and Guy Jacoby whose help has been indispensable (list was ordered by seniority...). Rona, special thanks for the devotion at which you performed the tasks I had too often asked you to help me with. I frequently trusted you more than myself with my own work! To Ram, the perfect F1 button whose computer work was so helpful. It may have even compensated for the many 'Ramcidents' you caused me. Guy, who stepped in to help with every purification and synchrotron run, but also stepped in with many interesting (and, well, time-consuming) physical discussions. I would also like to thank Steve Pregent, Yoni Messica, Ofer Doron and Ben Zuker who all participated in this work and the endless discussions it provoked. Far away from our home lab, I wish to thank to Michael Heymann for a very fruitful joint work during my stay in Brandeis.

I would also like to acknowledge the few biological 'mentors' I had during my PhD. Mostly, for helping me to like (or at least appreciate...) the biological work and biology itself. Yuval Reiss, thanks for your guidance and introduction to biochemistry. Your experience with proteins, which you enthusiastically shared with me, enabled much of the work presented here. To Harald Herrmann and Dorothee Möller, thank you for your great hospitality and excellent tutoring during my stay in DKFZ. I am mostly grateful for the many fascinating talks with Harald and the patient introduction of your valuable working procedures by Dorothee. And of course Adi: our lab manager and home-biologist. I am grateful for your biological perspective, which made everything more exciting. Even more importantly, thanks for your daily help at the lab and especially for maintaining its great working atmosphere!

I would like to thank Prof. Ekaterina Zhulina for her continuing interest and help in my work. Your detailed explanations, in discussions, papers and e-mails, were greatly

appreciated and considerably influenced this work. To Prof. Seth Fraden, for sharing his inspiring scientific scope and views during my stay in Brandeis University, and for great time I have spent at his lab. I would also like to thank Dr. Tomer Markovich, Prof. Yacov Kantor and Prof. David Andelman for useful suggestions and discussions. I especially thank David for one suggestion: to join Prof. Roy Beck's lab.

And last, I would like to thank my principle advisor, Prof. Roy Beck, who made all the above discussions, work and meetings possible. I sincerely appreciate the many efforts invested in introducing me to the field of biophysics. Also, in providing me with an ideal working environment: I never missed any piece of equipment or experimental technique at our lab. Thanks for supporting and encouraging my many trips to conferences, workshops and academic collaborators. Many thanks for the unimaginable availability for every deadline or question. I am also grateful for your support for my ideas and initiatives (the good as well as bad ones) and for sharing your creative research ideas and rare physical intuition.

Publications

1. E. Malka-Gibor, **M. Kornreich**, A. Laser-Azogui, O. Doron, I. Zingerman-Koladko, J. Harapin, O. Medalia, R. Beck, *Phosphorylation-Induced Mechanical Regulation of Intrinsically Disordered Neurofilament Proteins*, Biophysical Journal, 112(5) (2017).

2. T. Guterman, **M. Kornreich**, A.Stern, L. Adler-Abramovich, D. Porath, R. Beck, L.J.W Shimon, E. Gazit, *Formation of Bacterial Pilus-Like Nanofibers by Designed Minimalistic Self-Assembling Peptides*, Nature Communications, 7 ,13482 (2016).

3. **M. Kornreich**, E. Malka-Gibor, B. Zuker, A. Laser-Azogui, R. Beck, *Neurofilaments function as shock absorbers: compression response arising from disordered proteins*, Physical Review Letters, 117, 148101 (2016).

4. M. Storm, **M. Kornreich**, A. Hernandez-Garcia, I. Voets, R. Beck, R. de Vries, M.A. Cohen Stuart, F. A.M. Leermakers, *Loss of bottlebrush stiffness due to free polymers*, Soft Matter, 12, 8004-8014 (2016).

5. Laser-Azogui, **M. Kornreich**, E. Malka-Gibor, R. Beck, *Neurofilament assembly and function during neuronal development*, Current Opinion in Cell Biology, 32 (2015).

6. M. Storm, **M. Kornreich**, A. Hernandez-Garcia, I. Voets, R. Beck, M.A. Cohen Stuart, F. A.M. Leermakers, R. de Vries, *Liquid crystals of self-assembled DNA bottlebrushes*, The Journal of Physical Chemistry, 119(10), 4084-4092 (2015).

7. **M. Kornreich**, E. Malka-Gibor, O. Doron, A. Laser-Azogui, R. Beck, *Composite bottlebrush mechanics: α-internexin fine-tunes neurofilament network properties*, Soft Matter, 11, 5839-5849 (2015).

8. **M. Kornreich**, R. Avinery, E. Malka-Gibor, A. Laser-Azogui, R. Beck, *Order and disorder in intermediate filament proteins*, FEBS Letters, 589, 19, 2464-2476 (2015).

9. **M. Kornreich**, M. Heymann, S. Fraden, R. Beck, *Cross polarization compatible dialysis chip*, Lab on a Chip, 14(19), 3700-3704 (2014).

10. **M. Kornreich**, R. Avinery, R. Beck, *Modern X-ray scattering studies of complex biological systems*, Current opinion in biotechnology, 24, 716-723 (2013).

1 Introduction

A polymer is a large molecule composed of many covalently bound repeated subunits (Fig. 1.1). Naturally occurring polymers, such as rubber, were in use since prehistoric times even though they were not identified as polymeric.

The application of statistical mechanics to study polymers began in the 1930-1950's and sets the basis for polymer physics. The non-deterministic approach revolutionized the description of macromolecular structure and mechanics, and relied on emerging technologies in polymeric chemical synthesis for their experimental corroboration [3]. Later works by de-Gennes and des-Cloizeaux introduced scaling concepts into polymer science, and were thus able to provide more accurate predictions of semi-dilute solutions. There are, however, many facets of polymers for which our understanding is far from complete.

Polymer brushes (*i.e.* polymers end-grafted to a substrate) and charged polymers are two active research areas, which pose both experimental and theoretical challenges [4]. Most textbooks include very limited information about charged polymers [3, 5–7], and even less on polymers that contain both negatively and positively charged regions (*i.e.* polyampholytes) [8]. Modern review articles of these subjects still list multiple open

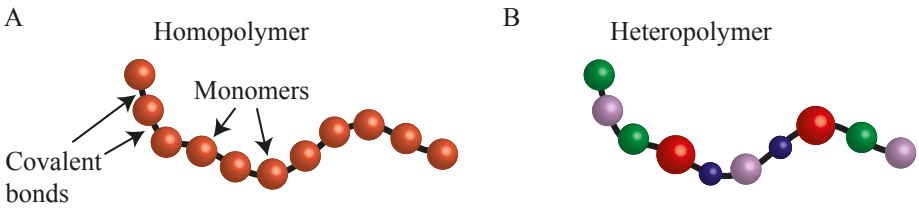

Figure 1.1: (A) A homopolymer is composed of multiple identical subunits (mer) chained by covalent bonds. (B) Heteropolymers consist of various monomeric units, which may vary in size, charge, hydrophobicity and more. Most biological polymers of interest, such as DNA and proteins, are heteropolymers.

questions [4, 9], provide limited predictions with respect to solvent conditions [8] and even lament the lack of sufficient experimental data [7]. The investigation of *grafted* charged polymers poses even greater challenges, which will be discussed below.

Charged polymer brushes are drawing increasing attention from the polymer physics community, not the least because of their proliferation in biology as well as their applicative medical and chemical potentials [10–12]. Theoretical studies predicted that charged brushes have a far richer mechanical and structural behavior than their neutral counterparts [13, 14]. However, the experimental investigation of these predictions was limited by the technical difficulty of synthesizing polymers which are not only sufficiently long to follow thermodynamic limits, but also very monodisperse (*i.e.* of the same size). On top of that, grafting of the polymers was made more complicated due to their strong electrostatic interactions.

In this thesis we exploit modern molecular biology tools to overcome these experimental obstacles, and to expose novel properties of charged and neutral polymer brushes.

Biological polymer synthesis was evolutionary perfected to produce extremely long polymers with outstanding reproducibility. Our increasing ability to harness this machinery holds great promises in biology, chemistry, medicine and polymer physics. For example, DNA is replicated with a breathtaking accuracy of 1 base pair error for every $10^5 - 10^8$ base pairs [15], which makes them an indispensable model system for *uniformly* charged polymers [6, 16].

Proteins, which are polyampholytes that also contain both hydrophilic and hydrophobic monomers, are far more diverse than DNA molecules. Consequently, much less is known about proteins (and polyampholytes in general [8]), owing to their unpredicted non-specific interactions with molecules and the solvent. Previous protein studies mostly focused on their folding into specific three-dimensional structures, which were thought to determine protein function. Remarkably, protein folding remains one of the biggest challenges of molecular biology to this day. However, the polymer physics community was less involved in this quest, since proteins did not adopt "polymeric" ensemble conformations [1]. Rather, they were thought to form a unique three dimensional structure that serves their functions. This view of protein functionality, relating function to specific structure, is being challenged in the past 20 years [1].

It is now believed that approximately 50% of human proteins contain long regions that are designed *not* to fold into any specific structure (see Fig. 1.2) . Instead, they assume

[1] For convenience, I will refer to proteins, which are heteropolymers, simply as polymers in this thesis.

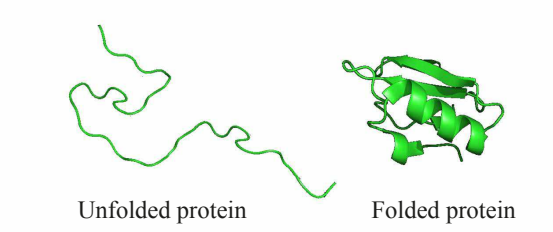

Figure 1.2: Protein folding. (A) An unfolded protein dynamically transitions from one conformation to another, and its contour can be described as random walk. (B) Under proper environmental conditions, many proteins fold into a stable or meta-stable specific three-dimensional structure. Proteins that contain large functionally important regions that do not fold are classified as IDPs.

a conformational ensemble which is crucial for their designated functions. The investigation of these proteins, known as intrinsically disordered proteins (IDPs), naturally calls for mechanical statistical tools[2]. In this thesis we will probe the structure and mechanics of IDPs by combining conventional soft matter characterization techniques with modern proteomics and genetic engineering. Most importantly, we will show that short-ranged electrostatic forces in polyampholytes have a far more versatile role than previously considered[3]. We will demonstrate how short-ranged interactions modify the osmotic stress response, expansion and macroscopic hydrogel orientation of polyampholyte protein complexes (see sections 2.1–2.4).

This thesis is organized as follows: in the reminder of chapter 1 the theoretical background and the biological systems used in our research are presented. These include neuronal intermediate filament proteins, which form a dense nematic hydrogel in axons. Chapter 2 presents our investigation of charged and neutral polymer brushes, and the development of a new microfluidic device essential for their future assembly studies. In chapter 3 I introduce three more papers completed during the course of this PhD. Finally, in chapter 4 I summarize our key findings and suggest future directions in the study of IDPs and polyampholytes.

[2] Notably, a protein which is mostly folded but also contains a long disordered (*i.e.* unfolded) region is included in the standard definition of IDPs.

[3] Short compared to the electrolyte size, where continuous electrostatic models of solvent polarizability and ionic screening do not apply.

1.1 Polymer brushes

Polymer brushes are polymers end-grafted to a substrate, which alter the supported surface's interactions and reactivity with its surroundings. Earliest physical models of polymer brushes date back to the late 70's, now collectively known as the Alexander de Gennes model [17, 18].

The Alexander de Gennes model [17, 18] considers neutral polymer brushes that interact sterically. It predicts a phase transition of polymer brush height in good solvent with increasing grafting density (σ). At low grafting densities, the brushes are in the so called mushroom regime (Fig. 1.3), where the distance $D = \sigma^{-1/2}$ between the anchoring points of neighboring grafted polymers is larger than the radius of gyration R_g of the polymer in the free solution. The brush layer height, denoted H, is comparable in this regime to the radius of gyration $H \sim R_g$ for a non-adsorbing surface.

As grafting density increases and $\sigma^{-1/2} \ll R_g$, polymers stretch and the brush height increases, known as the brush regime. For self-avoiding polymers, *i.e.* whose segments interact sterically, the brush layer height follows a linear exponent rule

$$H \sim L_0 w \sigma^{1/3}, \tag{1.1}$$

where L_0 is the length of a fully stretched polymers and w is the excluded volume parameter (Fig. 1.3B).

A similar scaling behavior can be derived for polymers grafted to a cylindrical substrate with radius is R [19]. Unlike in the planar Alexander de Gennes model, the volume fraction (Φ) is not uniform, but holds:

$$\Phi(r) \sim a^{4/3} r^{-2/3} \left(\frac{R}{D^2} \right)^{2/3}, \tag{1.2}$$

where a is the monomer size and r is the distance from the cylinder center. The brush height, assuming that all polymers are equally extended is[4]

$$H \sim \left(\frac{R}{D^2} \right)^{1/4} (L_0/a)^{3/4} a^{5/4} \tag{1.3}$$

Notably, the linearity with L_0, which held in the planar configuration, is lost.

[4] This Alexander de Gennes assumption was later shown to be problematic. A more accurate solution found that the brush volume fraction follows a parabolic profile and that the extension of the polymers in non-uniform [20].

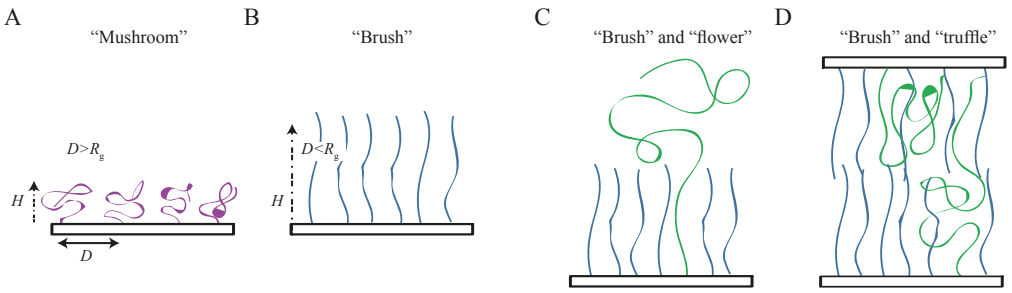

Figure 1.3: Schematic representations of the (A) mushroom and (B) brush regimes, the mixed-polymer (C) flower conformation and the newly introduced truffle regime. The (A) mushroom regime holds for $\sigma^{-1/2} < R_g$. With increasing grafting density, as $\sigma^{-1/2} \gg R_g$, the brush height scales with the grafting density $H \sim L_0 w \sigma^{1/3}$. A cartoon of the (C) flower conformation of two polymers with different grafting densities. At the inner corona, the short polymer and the grafted ends of the long polymers (coined stems) are well extended, while the at outer corona the free ends of the long polymers act as Gaussian or self-avoiding chains. Opposing mixed-polymer brushes with attractive interactions can inter-penetrate and form a collapsed "truffle" conformation (D), where the long polymer flower condenses into the short-polymer brush [24].

The brush organization can be altered by grafting a small fraction of long polymers (with N_1 monomers) in midst of the dense brush of shorter polymers (with N_2 monomers). In this case, the shorter polymers do not allow longer polymer interpenetration near the surface, and consequently the longer polymers are repelled farther away. This creates two layers. First, a brush-like packed region near the grafting surface, composed of the short polymers and tips of longer polymers, whose height holds $H_1 \propto N_1$. Second, an outer layer composed of long polymer ends, whose height holds $H_2 - H_1 \propto (N_2 - N_1)^{\nu}$ with $0.5 < \nu < 0.6$ (Fig. 1.3C). This two-layered organization is known as the flower conformation [21–23].

Polymer grafting is an efficient method of modifying surface interactions in biological, medical and industrial applications [11, 12]. When densely grafted opposing planar brushes are pressed against each-other, the compression response resembles that of a semi-dilute solution [18]. It therefore follows the des Cloizeaux result for a semi-dilute polymer solution, together with the elastic entropic tensions [25]:

$$\Pi(H) \sim \frac{k_B T}{D^3} \left[\left(\frac{H_0}{H} \right)^{9/4} - \left(\frac{H}{H_0} \right)^{3/4} \right]. \tag{1.4}$$

Here, H_0 equals H for $\Pi \approx 0$ and the pressure term applies to neutral polymers which

interact sterically.

However, many brush systems of interest are composed of charged polymers, *i.e.* polyelectrolytes. There, excess repulsion is formed by the ionic osmotic pressure and pair-wise Coulomb interactions [26, 27]. The latter are screened by counter-ions and added salts, and may be neglected when the electrostatic screening length is smaller than the average distance between charged monomers in the brush[5]. Then, the ionic osmotic pressure will be approximated by the Donnan equilibrium (for a detailed derivation see supplementary of section 2.3):

$$\Pi_{\text{ion}} = k_{\text{B}}T\left(\sqrt{c_e^2 + 4c_s^2} - 2c_s\right), \tag{1.5}$$

where c_e is the density of ionized polymer monomers, and c_s is the bulk salt concentration. Combining the ionic osmotic pressure (given by the first term in the r.h.s of Eq. 1.5) with the steric excluded volume interaction (Eq. 1.4) effectively equates the charged brush to an ideal counterion gas co-existing with neutral, end-grafted polymers.

The two limits of Donnan rule define two additional brush regimes: salted for $c_s \gg c_e$ and osmotic for $c_s \ll c_e$ [13, 14]. In the salted regime, the ionic osmotic pressure is $\Pi_{\text{ion}} = k_{\text{B}}T(c_e)^2/4c_s$, whereas in the osmotic regime it does not depend on the added salt concentration and holds $\Pi_{\text{ion}} = k_{\text{B}}c_e$. As grafting density and salt concentration increase, the brush can enter a quasineutral regime where the steric contribution to the pressure dominates and $\Pi \sim L_0\left(a^5/\sigma\right)^{1/3}$.

Additional complexity and opportunities are introduced when grafted polymers contain monomers that also engage in attractive interactions. For example, colloids grafted with negatively charged DNA polymers can form hydrogen cross-links between DNA segments. The location and strength of these cross-links are mutable, which can be exploited for controlling colloidal flocculation and aggregation kinetics [28]. Alternatively, surfaces can be modified by grafting complex neutral polymers. Neutral polystyrene brushes, whose non-grafted ends are modified to interact via a dipole-dipole interaction, considerably increase the shear between opposing grafted planes [29].

---

[5] In polyelectrolyte solutions, the electrostatic screening length is often taken as the Debye Length $\lambda_{\text{D}} = \left(\frac{8\pi c_{\text{ion}} e^2}{\varepsilon k_{\text{B}}T}\right)^{-1/2}$, where e is the electron charge, ε is the relative dielectric constant and c_{ion} is the free ion concentration in the brush. In fact, alternative screening lengths should be used at lower salt concentrations, which will not be discussed here [26].

1.2 Intrinsically disordered proteins

Disordered proteins bear considerable resemblance to the polymers described above: they take multiple co-existing conformations, and often contain segments which almost act as random-walk-shaped polymers (Fig. 1.2). It is now believed that approximately 50% of human proteins contain long disordered regions, and are therefore classified as IDPs. Mapping the functional roles of these regions and proteins as well exploiting their diversity to tackle open questions in polymer physics, is an on-going quest that joins biologists and physicists since the late 90's [1, 30]. In this section, we wish to review some of the inherent obstacles present in the study of IDPs.

Prior experimental evidence suggested that a combination of high net charge with low average hydrophobicity is a prerequisite of protein structural disorder [1]. The charge-hydrophobicity phase space separating ordered and disordered amino acid sequences was defined by the phenomenological boundary relation between the average hydrophobicity $\langle|\eta|\rangle$ and normalized mean charge $\langle|Q|\rangle$:

$$\langle|Q|\rangle = 2.785\,\langle|\eta|\rangle - 1.151 \tag{1.6}$$

As the characterization methods of IDPs were improved, a few exceptions to this simplified rule were found [1], as we will also discuss in section 2.2.

IDP characterization poses non-trivial challenges, since the ensemble conformation of IDPs denies the formation of long-range order, which naturally prevents crystallization. Consequently, Nuclear magnetic resonance and X-ray diffraction are incapable of providing an atomic-level snapshot of an IDP, which are available for folded proteins. Still, Nuclear magnetic resonance and small-angle scattering can identify IDPs and provide valuable information on their ensemble conformations and dynamic features. Alternative popular methods for the identification of IDPs include Förster resonance energy transfer (FRET) and Electron paramagnetic resonance, which can both target the dynamics of specific protein regions with the help of associated tags and chemical modifications [30]. Electron microscopy was specifically used to directly image the angstrom-thick IDP tails of NFs, but required pre-staining by high contrast metals due to the proteins' low electron contrast [31, 32]. The staining process considerably thickens the protein's main-chain, and therefore distorts the molecular details. The distortion is especially detrimental for the study of IDP complexes and dense solutions.

Given these experimental impediments, and in order to elucidate the design and function of IDPs, major efforts have been invested in computational investigations of IDP

structure. However, predicting IDPs conformations by simulation and free energy calculation is made complex by the heteropolymeric nature of proteins. Any protein is composed of multiple monomers, where each of the 20 available monomers differs in size, shape, polarity and charge. The interactions between different monomers typically depend on the atomic details, which must take neighboring monomers and solvent molecules into account. As all simulations apply some level of approximation and coarse-graining, it can be understood why their predictions remain imperfect. In fact, our own experimental results (presented in the following chapter) refute NF simulation predictions on several key issues.

Special theoretical and experimental attention was drawn to the characterization of the intrinsically disordered NF protein brushes, which are critical components of the cellular scaffold [33–38]. The resultant ample literature, detailed in section 1.4, poises NFs as a much-needed meeting point between current experiments and theories of IDPs.

1.3 The cytoskeleton

The cellular scaffold (*i.e.* cytoskeleton) is composed of three interconnected structures: the actin microfilaments, microtubules and intermediate filaments (IFs), Fig. 1.4. Actin microfilaments and microtubules filaments are composed of few folded proteins which are identical in all cells and tissues. In contrast, mammalian IF proteins are expressed by 70 different genes in a cell-specific manner, and conspicuously contain large and functional disordered regions. These have evolved to support the cellular distinctive mechanical needs, and therefore differ in size, amino-acid content and charge [39–41].

As we will later show (section 2.2), IF proteins form elongated filaments, while their intrinsically disordered solvated C-terminal regions radiate from the filament backbone (Fig. 1.4, top right). The disordered region, commonly referred to as tail, is especially long in neurofilament (NF) proteins, which are IFs of the nervous system.

1.4 Intrinsically disordered neurofilament proteins

The long flexible tails of NF proteins, which are the neuronal intermediate filament proteins, give rise to neurofilaments' known bottlebrush architecture (Fig. 1.5). NFs are the most abundant cytoskeletal components in axons, which are slender projections emanating from neuronal cells (Fig. 1.6). Mammalian axons are $\sim 50\ \mu$m wide and can extend to as much as 1 m in length [42]. This unusual aspect ratio is structurally supported by

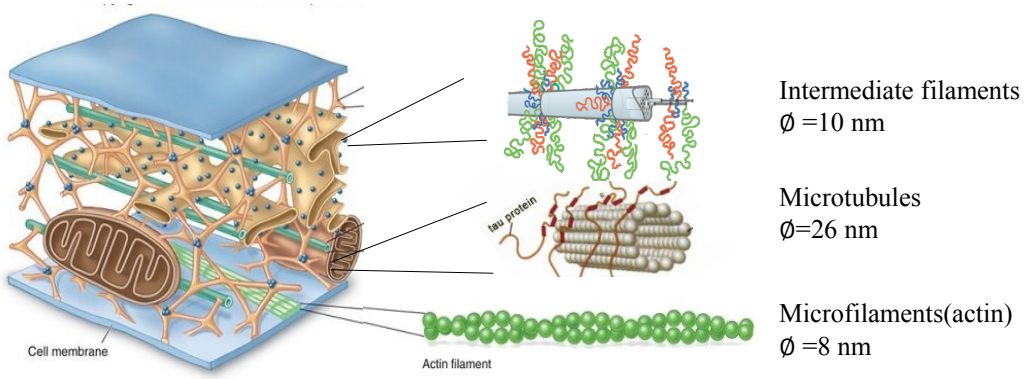

Figure 1.4: The cytoskeleton primarily gives the cell shape and mechanical resistance to deformation. It is also involved in multiple critical cellular functions, such as cell migration, endocytosis and cytokinesis as well as intracellular transport and organization [40]. The cytoskeleton is composed of three interconnected filamentous protein networks: actin microfilaments (diameter $\phi = 8$ nm), microtubules ($\phi = 26$ nm) and intermediate filaments ($\phi \approx 10$ nm).

the axonal well-aligned and organized cytoskeleton (Fig. 1.6B,C), whose interactions are affected by the disordered NFs tails.

NFs form composite filaments, consisting of four different proteins: NF-L (62 kDa), NF-M (103 kDa), NF-H (117 kDa) and α-internexin (α-Inx, 66 kDa). The key differences between the four proteins lie in their tail regions, which are distinctive in their lengths and amino-acid content (Fig. 1.5). Given their flexible nature, the tails can be treated as polymer brushes: flexible chains end-grafted to cylindrical substrates.

The pivotal role of the NF tails in the cytoskeletal organization, health and disease is evident from their involvement in neuronal development as well as neurodegenerative disorders [41]. Disorders which implicate genetic and enzymatic modifications of the NF tails include amyotrophic lateral sclerosis, Alzheimer's, Parkinson's and Charcot-Marie-Tooth [44]. During the normal course of neuronal growth and development, the relative molar ratios of the four NF proteins are altered to accommodate the changing needs of neurons [41]. Since the main differences between the NFs lie in their tail regions, understanding tail organization is key to understanding the roles of NFs in neuronal development and pathology.

Despite NF tails' established biological importance, a full description of their conformations and interactions is still missing. To our best of knowledge, the only available direct images of the NF tails were performed by either rotary shadowing transmission

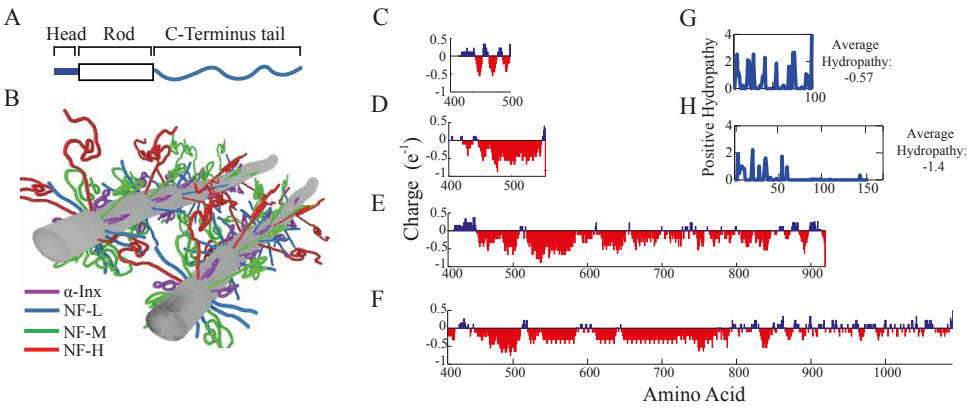

Figure 1.5: Subunit proteins form filaments that interact via polyampholyte C-terminal tails (adapted from [24]). (A) An illustration of a neural intermediate filament subunit includes a well-conserved central α-helical rod domain flanked by intrinsically disordered N-terminal head and C-terminal tail domains. (B) A schematic of interacting bottlebrush IFs composed of four different neuronal subunit proteins. (C-F) Tail charge distributions of (C) unphosphorylated α-Inx and phosphorylated (D) NF-L, (E) NF-M and (F) NF-H are calculated at pH=6.8 and averaged over a 5-amino acid window. The positive values of (G) α-Inx and (H) NF-L tail hydrophobicity index, summed with a 3-amino acid window, are plotted next to the overall hydrophobicity score, -0.57 and -1.4, respectively [43].

electron microscopy [32] or antibody labeling [31][6], both preceded by fixation and solvent dehydration. Such drastic procedures are expected to modify the organization of flexible protein regions - including the NF tails.

Several Monte Carlo and molecular dynamics simulations aimed at bridging this gap [34,49,50], and propose a detailed theoretical picture of the NF brushes (Fig. 1.7). Monte Carlo simulations of parallel opposing filaments reported increasing tail inter-penetration as NF were forced closer, and suggested that tail-mediated interactions are steric under physiological conditions [50]. The prominence of steric interactions over cross-bridging was ascertained by information analysis of NF network electron microscopy micrographs [35, 51]. In contrast, self-consistent mean-field calculations predicted considerable hydrophobic interactions between adjacent filaments that can form stabilizing cross-bridges between NFs [34]. They further predicted that the repulsive electrostatic forces, under physiological conditions, are comparable to the steric forces. In agreement, several exper-

[6] Subsequent experiments using cryo-electron-microscopy suggested that the observed cross-bridges were not necessarily the NF tails, but additional associated cross-bridging proteins [45] or even staining artifacts [46,47].

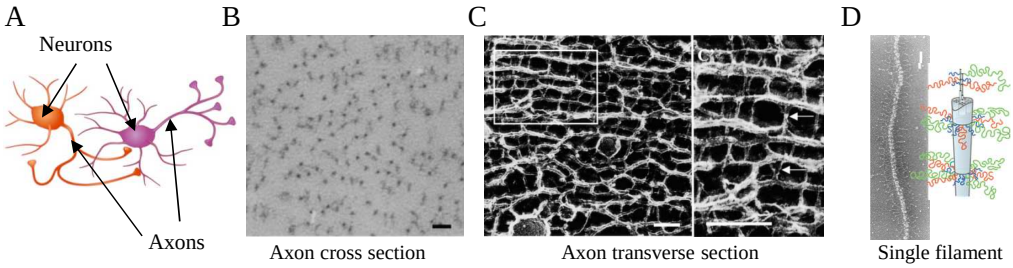

Figure 1.6: (A) Schematics of neurons with protruding, neurofilament-rich axons. (B) Quick freeze deep etch micrographs of the axonal cross section of sciatic nerves, showing multiple aligned neurofilaments. Scale bar 500 nm [45]. (C) Axonal transverse section (left) and higher magnification view (right). White arrows point at cross-bridges. Scale bar 200 nm [45]. (D) Rotary-shadowed view of a native neurofilament showing the tail domains of NF-M and NF-H extending from the core of the filament. Scale bar 100 mm [48].

imental studies including rheology, X-ray diffraction and atomic force-microscopy also noted considerable cross-bridging. However, these were attributed to electrostatic interactions, not hydrophobic [38, 52, 53].

Evidently, there are currently multiple contradicting views regarding NF disordered tail conformations and interactions. In this thesis the few discrepancies found between these studies and our experimental results will be addressed. Most importantly, we explain our results by considering strong short-ranged attraction between oppositely charged residues, which may be enhanced by counter-ion release (see chapter 2). The implicated bridging sites are identified using an electrostatic "toy model" and then directly verified by biological manipulation of the polymer brushes. The biological manipulation is achieved by tampering with the protein composition of the cylindrical filaments (section 2.1), by genetic engineering of specific monomers (section 2.3) and by enzymatic modifications of the polymer charge distribution (section 2.4). Moreover, we fit our osmotic compression data to a modified Alexander de Gennes model and conclude that at near physiological conditions the steric and electrostatic repulsive forces are comparable. Consequently, we find that the known biological charge modifications machinery, known as phosphorylation, can effectively change the NF network compression resistance and expansion.

1.4.1 Biological roles of neurofilament proteins

The most commonly considered role of NFs is to provide cells with structural support, which includes NF critical function in radial growth during development, in axon injury,

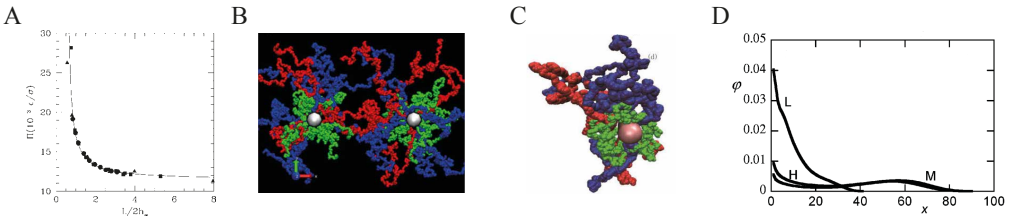

Figure 1.7: (A) Molecular dynamics simulations of two opposing planes, grafted with either NF-L (triangles), NF-M (squares) or NF-H (circles) [36]. The plot of the pressure Π as a function of normalized separation $L/2h_\infty$ is fitted with a $1/L$ line, where h_∞ is the brush height at infinite separation distance L. $\varepsilon/\sigma = 76$ kPa are Lennard-Jones parameters of equation 3 therein. (B) Monte Carlo simulation of two opposing cylinders, 60 nm apart, grafted with NF-L (green), NF-M (blue) and NF-H (red) tails. The flower conformation mentioned in section 1.1, as well as tail cross-linking are discernible [50]. (C) Alternative Monte Carlo simulations found that NF tails tend to fold back and adopt loop-like conformations [54]. (D) Numerical self-consistent mean-field calculation provide the overall radial volume fraction (φ) profiles of the tail monomers at different distances (x nm) from the cylindrical NF core [55].

and the maintenance of axon caliber [41, 56–58]. This is especially important in axons, where the transmission of electrical impulses along the axons is correlated to the axon diameter [59].

Studies of transgenic (genetically modified) mice suggest that NFs may have additional roles. These were conducted on mice that do not express at least one of the NF triplet proteins (NF-L, NF-M, NF-H) and of gene-replacement mice that express tailless versions of NF-M or NF-H have yielded puzzling results.

Deletion of the NF-M tail significantly reduced the axon caliber [60], while deletion of the longer NF-H tail appeared to have no affect on it [61, 62]. Surprisingly and in contrast to the hypothesized relation between conduction velocity of impulses and the axon caliber, mice expressing tailless NF-H did suffer a decrease in conduction velocity [62]. The authors deduced that this disparity between axon caliber and conduction velocity indicated that NF-H must have a non-structural role, and suggested that NF-H tail may affect the axon ion channels. However, this hypothesis was later disputed as it appeared that the disparity between axon caliber and conduction velocity disappeared in older NF-H tailless mice. Instead, it was found that the lack of NF-H tails slows down the radial growth of the axon distally along the nerve (*i.e.* away from the neuron body Fig. 1.6). Since the caliber was previously measured in the proximal regions only, earlier studies which reported the disparity may have been performed on mice whose caliber is actually modified in distal

regions along the axon [61, 63].

Studies on NF tail phosphorylation in transgenic mice also indicated that NFs may have additional functions which were not structural-mechanical, and are controlled by their phosphorylation[7]. For example, while it was thought that tail phosphorylation should increase the inter-filament spacing and resultant axon caliber, it was found that mice expressing mutated NF-M proteins incapable of tail phosphorylation have similar NF spacings and axon caliber to healthy mice [64]. As in the tailless NF-H mice, no compensatory expression of other cytoskeletal proteins or altered phosphorylation rates were reported [61, 64]. One possible alternative role of NF phosphorylation was that NF tail phosphorylation sites act as phosphorylation sinks that prevent excessive phosphorylation of other neuronal components [65]. Despite the ability of the NF tails to prevent hyperphosphorylation of the neuronal tau protein is now established, the biological significance of NFs as phosphorylation sinks remains unclear [66].

In section 2.4 we will reveal a possible new rationale for NF tail phosphorylation. We will show that NF phosphorylation has only a moderate effect on NF network expansion, but a more dramatic effect on its compression response. Moreover, in section 2.1 we will find that removal of either NF-H or NF-M from the mature network (which contains four NF proteins) has a negligible effect on the network structure and compression response. Therefore, removal of NF-M tail in transgenic mice is detrimental probably due to its other functions, such as interacting with other cytoskeletal components [68].

A structural role of NFs that will not be considered in this thesis originates from the binding between NFs and other cytoskeletal components and is critical to organelle distribution inside axons [67, 68] as well as their interaction with neuronal receptors [69]. NF phosphorlyation is expected to play a major role in these interactions [41, 68].

1.5 Bottlebrush and liquid crystals

Liquid crystal materials combine orientational ordering with the absence of long-ranged translational ordering, which poises them between solids and liquids. Many liquid-crystalline materials are composed of anisotrpoic rod-like particles, ranging from the nanometric to the micrometric scale. An orientational arrangement can sterically arise at high volume fraction (Φ), where it impossible to arrange the particles in an isotropic way (Fig. 1.8).

From this viewpoint, it is clear that stiff-chain macromolecules, that is, polymers in

[7] This is not to be confused with NF transport along axons or NF assembly, which are not to be considered as NF roles although they clearly depend on NF tail phosphorylation [41].

which the length l_K of a Kuhn segment is much greater than the characteristic thickness d of the polymer chain, should easily form a liquid-crystalline nematic phase[8].

In 1949, Onsager proposed the first molecular theory for a lyotropic nematic transition, which was valid for long, thin rods that interact sterically [71]. The free energy approximation is a functional of the distribution function of the rod orientations ($f(\mathbf{u})$),

$$F = NT\ln\Phi + NT\int f(\mathbf{u})\ln 4\pi f(\mathbf{u})d\Omega_u \tag{1.7}$$

$$+NTc\int\int f(\mathbf{u}_1)f(\mathbf{u}_2)B(\gamma)\,d\Omega_{u_1}d\Omega_{u_2}. \tag{1.8}$$

Here, N is the number of rods, c is their number density and $B(\gamma)$ is the second virial coefficient for two interacting rods which make an angle γ with each other. Minimization of the functional for rods of length L and diameter d predicts a first order phase transition at low volume fractions ($\Phi \sim d/L \ll 1$). The rods solution is isotropic for $\Phi < \Phi_i = 3.290d/L$, anisotropic for

$$\Phi > \Phi_a = 4.223d/L \tag{1.9}$$

and in co-existence phase for $\Phi_i < \Phi < \Phi_a$. This approximation holds well for stiff polymers where $l_K \gg L$. For more flexible polymers, L can effectively be replaced with l_K, which is proportional to the persistence length [6].

In bottlebrush polymers, the dense corona of side chains affects both the persistence length of the main chain and the effective diameter formed by the grafted side-chains (D_{eff}). Early theories suggested that the ratio between l_K and D_{eff} increases, and hence ultimately leads to lyotropic liquid-crystalline behavior [72]. However, recent theories and simulation suggest that $l_K \sim D_{\text{eff}}$, such that no liquid-crystalline behavior is induced by bottlebrushes [73].

In this thesis, we experimentally study the liquid-crystalline behavior of NF and charge-neutralized bottlebrushes[9]. We show that the effective aspect ratio of the latter, produced by coating a DNA polymer with long hydrophilic chains, is *reduced* by the bottlebrush coating (see section 2.5). We also report a counter-intuitive loss of chain-stiffening at high concentrations (see section 2.6). Together, the loss of main-chain stiffening at high concentrations and the aforementioned aspect ratio decrease indicate that bottlebrushes *disfavor* a nematic organization.

[8] Or cholesteric phase, if the particles are chiral [70].

[9] Studies on charge-neutralized bottlebrushes were conducted in collaboration with the Physical Chemistry and Soft Matter subdivision of Wageningen University, the Netherlands.

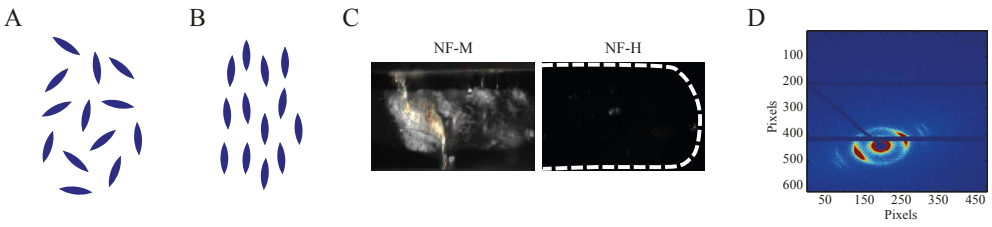

Figure 1.8: (A) An isotropic solution of particles lacks both orientational and translational order. (B) A nematic phase has an orientational order only, where particles are preferably aligned along a director vector. The alignment is observed by (C) cross-polarized microscopy: the nematic NF-M hydrogel appears illuminated (left), whereas the de-phosphorylated NF-H network is dark (right), indicative of an isotropic filament arrangement [74]. (D) Filament orientation can also be characterized by SAXS, where nematic samples scatter anisotropically [75].

1.6 Methods for soft matter characterization

This section introduces the main experimental techniques used in this work and emphasizes their applications and limitations for IDP research.

1.6.1 Small angle X-ray scattering

Wavelengths comparable to the size of atoms make X-rays ideally suited to reveal the structural details of macromolecules. The highly energetic photons primarily interact with the electrons of the target, resulting in elastic scattering. X-ray thus scattered by spatially correlated electron pairs constructively and destructively interferes in accordance to Bragg's law: $n\lambda = 2d\sin\theta$, which relates the distance d of parallel lattice planes with the scattering angle θ at a given wavelength λ and order n.

When macromolecules are randomly oriented in solution, all configurations are sampled during the experiment and the scattering profile is azimuthally symmetric around the primary beam. The scattering profile depends on the size and shape of the macromolecule.

In order to reveal structural information about shape and size of macromolecules in the length scale of several nm as for intermediate filaments, very small angles in the diffraction pattern have to be considered. SAXS measurements are typically concerned with scattering angles of 0.1 to 10°.

The scattering intensity $I(q)$ is the square of the scattering amplitude $F(q)$:

$$I(q) = |F(q)|^2. \tag{1.10}$$

The electron density of a single molecule characterizes its form factor $f(x)$, while the structure factor $S(x)$, is determined by the ordering of the scattering particles with respect to each other. Using the convolution theorem one can write:

$$F(q) = f(q)\,S(q)\,. \tag{1.11}$$

The scattering from an assembly of identical objects is conveniently decomposed into contributions from the structure of an object (form factor), and the contributions from the arrangement of those objects, captured by the structure factor. For example, the scattering pattern of an isolated filament sets the form factor of the NF hydrogel, which is composed of multiple filaments. The correlation *between* filaments in the hydrodel is captured by the structure factor, which is expected in this case to take a Lorentzian shape [76].

In practice, NFs' radius are non-identical, and the form factor cannot be experimentally determined to find the structure factor and inter-filament correlation. Instead, an empirical procedure for the derivation of the Lorentz-shaped structure factor is used (see section 2.1 and Refs. [53, 77]). To obtain the inter-filament spacing, two-dimensional diffraction scattering data is collected from neurofilament hydrogels contained in quartz capillaries. It is integrated azimuthally, and the intensity is plotted versus the reciprocal distance q. A broad peak with a maximum in the range of $q = 0.1 - 0.2\text{nm}^{-1}$, whose magnitude and q position depend on subunit composition, osmotic pressure and volume fraction of protein, is observed [53, 77]. The peak is fitted with a Lorentzian function to extract the corresponding inter-filament spacing $d = 2\pi/q$. Broadening of this peak is observed due to density fluctuations and the semi-flexible nature of the individual filaments.

1.6.2 Cross-polarized microscopy

Cross-polarized microscopy (CPM) is a useful tool for the investigation of orientational order and therefore of liquid crystals (see also section 1.5 and Fig. 1.8C). This is accomplished by illuminating the sample with a linear-polarized light, while imaging with a polarization perpendicular to both the illuminating light and its propagation director. In an anisotropic sample, the phase velocity of the propagating light will depend on its polarization, which will consequently rotate the polarization of the incident light.

For example, let us consider a liquid crystal with refraction indexes $n_x \neq n_y$. A linear-polarized electric field $\mathbf{E}_{\text{inc}} = \mathbf{E}_{x',0}e^{i(kz-\omega t)}$, whose polarization $\hat{x}'$ is in the xy plane, illuminates the sample. Assuming a α angle between x and $\hat{x}'$, the polarized field can be

written as:

$$\mathbf{E} = \begin{pmatrix} E_x \\ E_y \end{pmatrix} e^{i(kz-\omega t)} = E_{x',0} \begin{pmatrix} \cos\alpha \\ \sin\alpha \end{pmatrix} e^{i(kz-\omega t)} \tag{1.12}$$

While travelling through the sample a phase of $\Delta\varphi = 2\pi d(n_x - n_y)/\lambda$ is accumulated, where d is the sample's width and λ the field's wavelength. Therefore the electric field after the anisotropic media is:

$$\mathbf{E} = E_{x',0} \begin{pmatrix} \cos\alpha \\ \sin\alpha \cdot e^{i\Delta\varphi} \end{pmatrix} e^{i(kz-\omega t)} \tag{1.13}$$

Transformation to the $x'y'$ coordinate system, which lies in the xy plane, shows that the electric field after the sample has a non-zero y' component if $e^{i\Delta\varphi} \neq 1$. Therefore, only materials with an anisotropic refractive index appear illuminated under CPM.

NFs hydrogels have a rich liquid-crystalline behavior, which depends on salt concentrations, protein content and enzymatic modifications (see sections 2.1, 2.3 and 2.4 and Refs. [53, 77, 78]). As described in section 1.5, the liquid-crystalline behavior of NFs and bottlebrush polymers in general, is not fully understood. Their time-resolved investigation at different conditions is made complex by the self-assembly process of the NFs, which requires dialysis.

Typical dialysis devices use hundreds of micro-liters, and therefore necessitate a considerable amount of often expensive proteins. This bulk requirement limits the experimentalist's ability to investigate the NFs' rich phase diagram, which involves salt concentrations, enzymatic modifications, protein concentrations and osmotic pressure. Moreover, dialysis devices are incompatible with CPM due to the anisotropic nature of the membranes used. Therefore, following the dialysis process, samples need to be transferred to CPM-compatible capillaries for imaging. This additional step limits the ability to reuse the sample for future experiments, and complicates the investigation of reversibility and hysteresis.

The utilization of microfluidics, which reduces the necessary volumes down to few micro-liters, can help overcome these impediments. In section 2.7 we developed a novel CPM-compatible dialysis microfluidic device, optimized for time-resolved studies of birefringent materials. It enables rapid buffer exchange with simultaneous dynamical CPM measurements as well as easy sample reuse[10].

[10] Succesful NF assembly can be performed by rapid buffer exchange [79].

1.6.3 Atomic force and electron microscopy

Atomic force and electron microscopies provide direct imaging of nanometric features of bio-polymeric complexes, as opposed to diffraction data obtained by SAXS, whose interpretation requires Fourier transform analysis. This sets atomic force and electron microscopies as natural complementary tools in for SAXS. We monitor the morphology of the individual filaments that make the NF hydrogel (see Fig. 2 in section 2.1), and verify the formation of elongated 10 nm-wide which resemble the native filaments. However, atomic force and electron microscopies are unable to obtain the gentle molecular details of the disordered regions due to their inherent resolution limitations or intrusive sample preparation procedures. Preparations include sample dehydration and either chemical fixation, staining or both (depending on the specific techniques employed). Consequently, the gentle molecular details of the disordered regions are lost and only the nanometric features can be discerned.

For detailed protocols on NF sample preparation for atomic force and electron microscopy, refer to the Appendix.

1.6.4 Protein expression and purification

The emergent IDP field opens another door for polymer physics and biology cross-talk. IDPs are exemplary diverse polymers, containing monomers which can be either polar or non-polar, and can also carry a negative or positive charge. To harness this diversity, one must be familiar with modern bio-molecular tools for the production, purification and modification of proteins.

In this thesis we develop and optimize protocols for the production and manipulation of NF IDPs of bacterial and mammalian sources[11]. This simultaneous work on different protein sources allows us to exploit their respective research advantages.

The main advantages of bacterial protein production are the high protein yield and the ability to genetically modify the protein sequence. For example, in section 2.3 we selectively remove protein segments to prove their cross-linking functions. The key benefit of mammalian purification is that extracted proteins include all biologically relevant enzymatic modifications, which are not present in bacterially produced proteins (see section 2.4). These modifications can be exploited to understand the role of electrostatics and steric forces in the polyampholyte polymers. Another notable advantage of non-bacterial

[11] Other bio-molecules used were obtained from our collaborators, including viruses (section 2.7), DNA molecules and bio-mimetic IDPs from yeast source (section 2.5).

sources is their superior protein production mechanisms, which enable them to fabricate much longer and more diverse proteins.

For detailed protocols on NF protein expression and purification, refer to the Appendix.

2 Main thesis papers

This chapter includes 7 papers which encompass the main work performed in the course of this PhD. The papers are not chronologically ordered. Instead, they are ordered to facilitate a clear, continuous, presentation of the thesis. The chapter can be divided into two parts: in sections 2.1–2.4 we investigate the mechanical and structural properties of intermediate filament networks, which act as a model system of polyampholyte brushes. In sections 2.5–2.7 we focus on the orientational ordering of bottlebrush polymers, and develop a novel cross-polarization compatible microfluidic device to facilitate their future investigation. Each section is dedicated to a single paper and is preceded by a short introductory text that places it in context of the thesis as a single research project.

2.1 Composite bottlebrush mechanics: α-Internexin fine-tunes neurofilament network properties

Neurofilament bottlebrushes consist of several neurofilament proteins, whose protruding tails differ in length, charge and charge distribution (see Fig. 1.5). At high-density, the bottlebrushes filaments form a nematic hydrogel through tail-mediated interactions. Recent studies have focused on the two largest neurofilament protein tails (NF-M and NF-H). Those studies found correlations between the expression levels of the long-tail NF proteins to the axonal architecture as well as the inter-filament spacing [22, 50, 56, 80].

In this paper we examine the mixed NF polymer brushes, and focus on the roles of the short-tailed NF proteins (NF-L and α-Internexin). This is achieved by modifying the protein, and therefore tail, composition. Surprisingly, we find that replacing NF-L with α-Internexin, whose tail is shorter and less charged than NF-L's, results in network *expansion*. Our experimental findings are explained by an ionic-bridge model taking into account the specific charge heterogeneity of each polymapholyte protein tail (Fig. 5 and Ref. [53]). This model captures the essence of the interactions leading to the observed non-trivial hydrogel properties, where short neutral brushes induce network expansion (Fig. 7).

2.2 Order and disorder in intermediate filament proteins

One of intermediate filament (IF) proteins primary roles is to form a stress-responsive scaffold inside cells. In the course of our work on NFs we took part in several studies involving other IFs such as vimetin, lamins and desmin. While these IF proteins are expressed in different cells or different cellular regions, they all contained a disordered C-terminal tail. As the interactions between IFs are thought to be tail-mediated, we suspected that disorder is crucial for the cellular structural or mechanical integrity. To examine this assumption over the large IF protein family, which contains over 70 proteins, we partook in a sequence-based analysis of IF disorder.

The Human Genome Project, completed in 2003, identified and mapped all the genes of the human body, including the 70 genes encoding for IF proteins (Fig. 1). We investigate IF protein sequences by their amino-acid content for biophysical properties (*e.g.*, charge, size and hydrophobicity) as well as by two machine-learning predictors of structural disorder. Most importantly, we find that disorder is the universal common denominator of the head and tail regions of IFs (Figs. 4 and 5). However, the two regions differ from one another in their solvent accessibility, resulting in dissimilar conformations: a buried head (*i.e.* hidden in the filament core) against a solvated protruding tail. These divergent conformations agree with their speculated structural roles: the head is directly involved in filament formation, whereas the tail is engaged in interactions with the filament surroundings.

To facilitate the exploration of the data and analysis we prepared a complementary graphical user interface, available at: `http://www6.tau.ac.il/beck` under *Resources*|*Software*.

2.3 Neurofilaments function as shock absorbers: compression response arising from disordered proteins

The evident preference of disordered proteins in the construction of cellular scaffolds, detailed in section 2.2, raises an immediate question: what is the physical rationale behind the biological architecture? To answer this, we measure and compare 200 samples which differ in tail length, charge, osmotic pressure, stoichiometry, and ionic strength.

To ascertain the role of electrostatic cross-bridges, as proposed in section 2.1, we identify and modify a suspected cross-bridging site on the NF-L tail (see Fig. 1). The identification is based on the electrostatic analysis performed in section 2.1 and ref. [53], which was aimed at locating potential electrostatic cross-bridging site. In agreement with our analysis, the genetic modification significantly reduces the magnitude of the attractive forces and supports the conjecture made regarding the role of electrostatic bridging in setting the inter-filament spacing. We hold that similar short-ranged attractions between oppositely-charged monomers must be considered in all future studies of dense polyampholyte polymer solutions and brushes.

Furthermore, to determine the long-debated roles of steric and electrostatic repulsions in setting the inter-filament spacing, we apply a modified Alexander de Gennes compression model to our experimental data of the polyamphlyte, non-planar NF networks. The fitting shows that the electrostatic repulsion is non-negligible at physiological conditions, as was argued by some authors (see Ref. [34] vs. Ref. [35]). At no compression, the polyelectrolyte model is corrected by a semi-quantitative attractive term which captures the entropic contractile tension that depends on the tail cross-bridging locations and multiplicity.

From the biological and material science perspectives, our results and analysis demonstrate the main advantages of polymeric (*i.e* unstructured proteins) building blocks. Polymeric solutions are less subjected to damage under large deformations, in comparison to solids and structured proteins. The osmotic response of the disordered proteins, which we modeled by ionic osmotic pressure and second virial excluded volume, resembles that of a pressurized gas. This is especially important in the axon, where large organelle transport and axonal flexibility require both a soft and elastic scaffold [81]. The employment of transient (attachable-detachable) cross-links, as demonstrated here, enables the deformation and reformation of the network [82, 83]. The binding is facilitated by the large conformational space explored by the disordered tails.

Nonetheless, we conclude the paper with two remaining unresolved issues. First, the proposed model inexplicably fails at physiologically irrelevant salt concentrations below

100 mM. Second, we observe an unexplained loss of orientational ordering in NF networks that had been modified to have less cross-bridges. These two issues call for more detailed theoretical work and could also benefit future experiments in simpler systems (see sections 2.5 and 2.6 which focus on bottlebrush nematic organization).

2.4 Phosphorylation-induced mechanical regulation of intrinsically disordered neurofilament protein assemblies

The role of electrostatic interactions in NF network, which we treat as a polyampholyte model system, has been long debated (see section 1.1). First, it is unclear whether the origin of the tail-mediated repulsive forces between NFs are primarily steric or electrostatic at near physiological conditions, *i.e.* ~ 150 mM added salt (see refs. [51] and [84]). Second, while most authors agreed that adjacent filaments are cross-bridged [38], the nature of the driving attractive interactions was disputed (hydrophobic, electrostatic or both [34]).

The NF tails' electrostatic charge is regulated by naturally occurring, yet controlled, extensive enzymatic addition of many negatively charged divalent phosphate groups. We exploit this machinery, known as phosphorylation, to manipulate the tails' charge and characterize their electrostatic repulsive and attractive interactions.

Our results show that the electrostatic repulsion, manifested by ionic osmotic pressure (see section 2.3), is comparable to the steric one. Therefore, the network mechanical response and expansion are tunable by phosphorylation charge regulation. Importantly, the addition of excess charge to the already negatively charged tails results in either network expansion or *collapse* (Fig. 4). The latter is surprising, since phosphorylation increases the already overwhelmingly negative charge of the tails (see Fig. 1.5), and was thus expected to expand the network. We explain this trend by the electrostatic cross-bridges formed by the phosphate groups. We provide a lower bound for the cross-bridging energy, estimated at $8\ K_{\mathrm{B}}T$.

Finally, we find that tail phosphorylation tunes additional macroscopic properties of NF hydrogels, such as network orientation and mechanical response to osmotic pressure. Similar manipulation of macroscopic protein network properties due to phosphorylation was not reported before. These call for further theoretical investigation, since the liquid-crystalline behavior of bottlebrushes is not fully understood. This is pursued in our collaborative research on the liquid-crystalline behavior of neutral bio-mimetic bottlebrushes, presented in the following sections (2.5 and 2.6), as well as in the development of novel experimental tools (section 2.7).

2.5 Liquid crystals of self-assembled DNA bottlebrushes

One of the puzzling findings of this PhD is the nematic-isotropic phase transitions of NF bottlebrushes (see sections 2.3 and 2.4). On the one hand, NF-H containing networks are isotropic at low salt concentrations, suggesting that electrostatics destabilize the nematic organization. On the other hand, enzymatic charge removal in NF-H tail also induces a transition from nematic to isotropic, indicating that charge stabilizes the nematic phase. Unfortunately, the liquid-crystalline behavior is poorly understood even for the simpler, neutral, bottlebrushes.

We therefore partake in a collaborative project aimed at elucidating the nematic organization of neutral bottlebrushes. We measure the effective diameter and nematic transition of semi-flexible DNA molecules coated with 400 amino acid long diblock protein polymers. We show that grafting long linear side chains leads to a reduction of the effective aspect ratio, at grafting densities relevant for neurofilaments. This affirms the theoretical predictions made by our collaborators [73], which contradict previous theoretical works [72]. This result may explain the loss of NF orientational order at low salt concentrations, where the brush height increases [53].

2.6 Loss of bottlebrush stiffness due to free polymers

In the following paper we investigate bottlebrush anisotrpic organization under molecular crowding (*i.e.* in the presence of surrounding free polymers). Using SAXS, we note that the alignment of crowded bottlebrushes does not increase with increasing osmotic pressure, as expected. Instead, the X-ray correlation peak of the crowded bottlebrushes widen with increasing osmotic pressure. This is not observed for uncrowded bottlebrushes (see figure 3 therein).

To explain these experimental observations, our collaborators performed molecularly detailed self-consistent field calculations. The calculations show that both the main DNA chain persistence length (l_p) and brush height (D) decrease with increasing free polymer concentrations. However, when the free polymer volume fraction equals that of the brush, the loss of polymer stiffness is more pronounced. Consequently, the aspect ratio l_p/D decreases with increasing free polymer concentrations. This may explain why molecular brushes rarely organize anisotropically, and why biological bottlebrushes, such as NFs and Aggrecan, are key components of lubricating and stress-responsive constructs.

2.7 Cross polarization compatible dialysis chip

We develop a microfluidic dialysis chip optimized for cross polarization microscopy. The design is relatively easy to implement for a variety of time-resolved experiments and creates new opportunities where sample quantities are limited and multiple environmental conditions (*e.g.* ionic strength, osmolytes, denaturants, *p*H, and enzymes) need to be accurately controlled and altered, as in the NF case.

The applicability of the device is demonstrated by using micro-liter amounts of fd virus as a model system. Our results show time scale separation between fast nematic director reorientation and slow phase separation (nematic-isotropic) involving mass transport. This device is key for a reproducible, accurate and rapid investigation of systems such as the NFs and charged-neutralized bottlebrushes, whose sizes are comparable to the micro-meter long fd viruses.

3 Additional papers

In this chapter we present an additional co-authored paper, which does not focus on IDPs, as well as two review papers.

3.1 Peptide self-assembly as a strategy for mimicking a bacterial pilus nanofiber

Understanding and controlling protein supramolecular assembly is not only challenging, given our limited understanding of protein-protein interactions, but also highly rewarding: protein complexes are inherently bio-compatible and bio-functional. In this paper, the key peptide segments responsible for a biological complex protein construct were identified and synthetically reproduced. The synthetic peptide, which combined two selected segments from the naturally-occurring pilin protein, self-assembled into ordered nanofibers. These were characterized by electron microscopy as well as X-ray diffraction and circular dichroism for secondary structure.

3.2 Neurofilament assembly and function during neuronal development

NF expression patterns significantly vary during the organism's growth and development, to accommodate the changing mechanical and structural needs of the nervous system. Since the key differences between the various NF protein lie in their disordered tails, our review offers a biophysical perspective that emphasizes the role of IDPs in governing the organization of NF network during development.

3.3 Modern X-Ray scattering studies of complex biological systems

Structural characterization of biological samples by X-ray scattering requires no sample fixation, tagging, markers or any other modifications. We review recent advances made in X-ray studies of biological samples, including the introduction of modern coherent X-ray sources; implementation of machine-learning algorithms for scattering analysis; and hybrid approaches that combine X-ray data with higher (*e.g.* NMR) and/or lower resolution (*e.g.* optical microscopy) techniques.

4 Discussion

In this thesis I experimentally investigated mechano-structural aspects of polymeric solutions, including polyampholytes and bottlebrushes. This was pursued by using a diverse set of bio-molecules, including viruses, NF proteins of bacterial and mammalian sources as well as bio-mimetic viruses composed of DNA and yeast-produced proteins.

We have shown that under large compression and high ionic strength, the largely negatively-charged *polyampholyte* NF tails can be well-approximated by uniformly charged tails. At low to moderate compression, the polyampholyte character of the tails is revealed and is manifested in dominant electrostatic cross-bridges.

The complex liquid-crystalline behavior of neutral synthetic bottlebrushes and that of NFs was investigated. We found that the aspect ratio of the neutral bottlebrushes decreases with grafting, and therefore disfavors a nematic organization. The NF liquid-crystalline behavior is more puzzling, since both reducing the tails' charge (which reduces the electrostatic interactions) and decreasing the ionic strength (which increases these interactions) interfere with the anisotropic organization.

This chapter overviews the main results and conclusions outlined throughout this thesis, and also provides a wider perspective which emphasizes their implications and relation to current theoretical works. I will also review remaining open questions that, in my opinion, will benefit from future experimental and theoretical work.

NF bottlebrush compression

NF compression response was investigated in sections 2.1, 2.3 and 2.4 and in previous works [53, 85]. Under considerable compression, the largely negative charges were successfully approximated as a superposition of a neutral brush co-existing with an ideal gas of free ions, at least at the high salt limit (section 2.3). This implies that neglecting the steric interactions, as commonly practiced in polyelectrolyte brush studies [10, 86],

is ill-advised in similarly charged polymer systems. Rather, it appears that the steric interactions are comparable to the ionic osmotic forces, as we verified by experimentally changing the salt concentrations (see section 2.3).

It is possible that the steric contribution is often overlooked since the osmotic pressure of both superpositioned systems (*i.e.* the neutral semi-dilute polymer solution and the ideal ionic gas) grows roughly quadratically with the polymer concentration. The osmotic pressure of a neutral polymer semi-dilute solution grows as the monomeric concentration squared times the monomeric excluded volume (section 2.3 and Ref. [3])[1]. Similarly, the ionic osmotic pressure, as given by Eq. 1.5 at the high salt limit, also grows quadratically with the polymer charge (c_e). Therefore, if the charge per polymer is fixed, the ionic osmotic pressure must also grow quadratically with the polymer concentration. Consequently, studies which only consider the scaling behavior of charged polymer compression may mistakingly attribute the quadratic increase to the ionic osmotic pressure alone.

A non-scaling approach was followed in section 2.3, where we applied an experimentally-derived persistence length of IDPs to calculate the steric repulsion[2]. A more elaborate non-scaling calculation at 150 mM monovalent salt derived theoretical NF-LMH compression profiles, presented in Figs. 6-8 in Ref. [34] (in terms of free energy per 0.6 nm of filament backbone). Corresponding osmotic pressure curves were produced from theses profiles using $\Pi = -\partial F_{\text{int}}/\partial V$, where V is the volume per filament. The calculated profiles yielded lower osmotic pressures and shorter inter-filament distances than those experimentally observed (Fig. 4.1). Disregarding the large inter-filament spacings (above 40 nm), an overall reasonable agreement for the compression response was obtained.

The considerable disagreement at large inter-filament spacings, above 40 nm, may originate from a non perfectly aligned organization of the filaments[3]. Alternatively, the discrepancies could also arise from the Flory interaction parameters which were used for the self-consistent mean-field calculation (see Table 2 in Ref. [34]). These parameters could now be revised using our new experimental data, and be applied to other IDP systems as well.

Monte Carlo and Molecular dynamic simulations are naturally another non-scaling tool for the investigation of NF networks, and hence can also help differentiate the steric and electrostatic contributions to the compression behavior. However, to our best of

[1] The osmotic pressure of semi-dilute solutions is actually expected to grow as $c^{9/4}$ or $c^{2.3}$, depending on the exponent of the self-avoiding walk: 0.6 or 0.588 exponent, respectively [3].

[2] A scaling approach was only applied for the attractive force, whose prefactor was anyway a fitting parameter.

[3] As suggested by Ekaterina Zhulina, private communication.

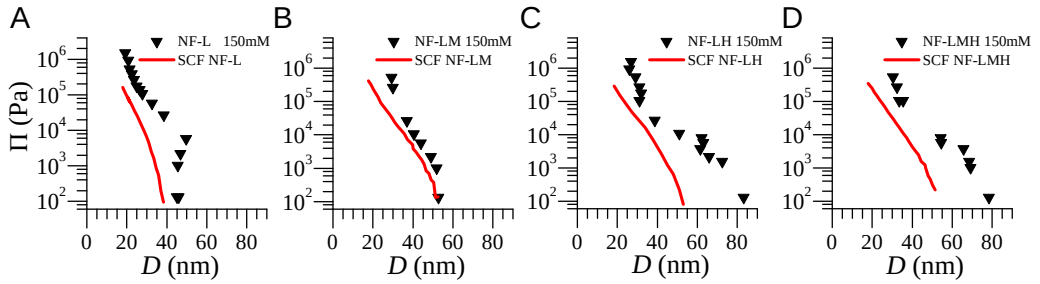

Figure 4.1: Self consistent mean-field (SCF) calculation of osmotic pressure (Π) vs inter-filament distance (D), compared to our experimental results. The SCF free energy calculation is described in Ref. [34] and the solid red line presented here is derived from the free energy F using $\Pi = -\partial F_{\text{int}}/\partial V$. The osmotic curves of (A) NF-L, (B) NF-LM and (C) NF-LH networks are provided through the courtesy of Prof. Ekaterina Zhulina. Their free energies were calculated as described in Ref. [34] for (D) NF-LMH networks (see "no cross-bridging" in Fig. 8 therein).

knowledge, no simulation study of NF compression response at comparable spacings was performed.

Notably, the non-negligible steric contribution which we report should affect polymer solutions in general, and is not limited to polymer brushes and polyampholytes. Instead, the steric interactions should also affect the compression response of semi-dilute polyelectrolyte solutions, and will become more pronounced at high ionic strengths ($c_s \gg c_e$ in terms of Eq. 1.5).

A simple experiment, which can directly probe the magnitudes of steric and electrostatic contributions in IDPs without requiring further analysis, can be devised using our available protein expression techniques (section 1.6.4). The disordered tail segment of NF-L alone was previously produced and purified at our lab using recombinant bacterial expression [87]. One could form a semi-dilute solution of the tails alone, and manipulate the net charge by altering the *p*H level. The resultant empirical excluded volume values should be compared to the values used in this study, which were based on amino-acid volumes of *folded* proteins (section 2.3 and Ref. [88]). While these values yielded reasonable agreement with our experimental compression data, their optimization could improve future predictions for concentrated IDP solutions and brushes [89, 90].

The inexplicable failure of the brush models used in section 2.3 to describe the compression response at low salt concentrations (below 100 mM) may be related to the approximation used. The disagreements are not related to the lesser orientational order of

the filaments, since NF networks are nematic at $\Pi > 10^4$ Pa, even at low salt concentrations [77]. While we would have like to compare these results to NF simulations, no theoretical prediction of the compression response of NFs at these salt concentrations is currently available[4]. However, alternative models which depict the expansion of polyelectrolyte cylindrical brushes are available [91, 92]. These may be expanded to provide the missing compression response predictions at low ionic strengths, which will go beyond the mean-field electrostatic approximations used. Namely, future modeling efforts should account for the Coulomb pair-wise interactions and consider the non-uniform distribution of the free ions in the brush.

Alternatively, the discrepancy between our low salt compression response and polyelectrolyte models could emanate from a meta-stable state. In other words, it is possible that the NF spacing is kinetically trapped while the osmotic pressure increases. Examining this possible explanation would require further experimentation. For example, NF hydrogels could be equilibrated at high ionic strength and then reequilibrated at low ionic strength, while maintaining a fixed osmotic pressure.

NF cross-bridging interactions

While this thesis emphasizes the role of electrostatic cross-bridges, it should be noted that the very existence of NF cross-bridging is still being debated. Previous molecular dynamics simulations [49] and data analysis of axonal cross-section micrographs [35, 46, 47] all argued that NF-tail attractive interactions do not significantly alter NF organization. In contrast, other studies suggested a pivotal role of attractive forces, and tail cross-bridging in particular. The cross-bridging hypothesis was first introduced and promulgated by Hirokawa and colleagues, based on electron microscopy studies of the frog axon. There, sidearms were found to form a dense network of cross-bridges that were 4-6 nm in diameter and 20-50 nm in length [93]. However, subsequent studies questioned these results and argued that the cross-bridges were only "artifacts" arising from the electron microscopy methods [46, 47].

Later support for the cross-bridging hypothesis was provided by rheology [38, 94], SAXS [24, 53], atomic force microscopy experiments [52], extensive NF bundling in neurons [95, 96] as well as the stable phase separation of NF filaments [77]. Nonetheless,

[4] The only available theoretical prediction of NF compression response at low salt concentrations appears in Ref. [34], using a mean-field model. These include the NF-LMH network only, which we did not measure at low ionic strengths. However, these were measured in Ref. [53] and do not agree with the predictions of Ref. [34].

these studies, which all agreed on the existence of NF cross-bridges, suggested different cross-bridging mechanisms: either electrostatic, hydrophobic or by associated proteins.

To provide a *direct* proof of the existence, nature and importance of electrostatic cross-bridging, we reverted to the biological toolbox described in section 1.6.4, and manipulated the tail charges using genetic and enzymatic modifications. The removal of the short NF-L positive C-terminal tip proved its key role in setting the inter-filament spacing and orientational order of NF-L and NF-LM networks. As the tip segment includes no hydrophobic amino-acids, this result is attributed to attractive electrostatic interactions (section 2.3).

Another experimental demonstration of NF tail cross-bridging, and electrostatic in particular, was provided in section 2.4. There, we enzymatically modified the NF-M and NF-H tail charges, which resulted in an unexpected expansion of de-phosphorylated NF-LM brushes. This, again, indicated that the negatively charged phosphates were involved in attractive interactions. Comparison of the compression curves of phosphorylated and de-phosphrylated NF-LM networks provided us with a lower bound for the attraction energy per phosphate, estimated at 8 $k_{\mathrm{B}}T$, which was comparable to the binding energy of salt bridges [97]. Our calculation provides, to our best of knowledge, the first experimental estimation of the electrostatic binding energy per NF phosphorylation site.

The experimental identification of protein binding-sites is crucial not only for our understanding of NF tail-tail interactions, but also for elucidating IDP and polyampholyte interactions in general. For example, an inaccurate estimation of the binding energies may explain the disagreement of recent theoretical predictions with our experimental results. For example, we found that replacing NF-L with α-Inx expands NF networks (section 2.1), contradicting previous theoretical predictions [22]. Furthermore, we showed that phosphorylated NF-M tails are less extended than the de-phosphorylated ones in NF-LM network, which did not agree with the expanded phosphorylated NF-M tail conformation predicted by simulations (Fig. 1.7). It is possible that inclusion of tail-tail electrostatic cross-bridging energies in the simulation could have improved these predictions (and those of IDPs and polyampholytes in general). Such free energies are commonly considered in the study of salt-bridges in crystallography. Their calculation includes the free energies of counter ion release and the Coulomb interaction, which both contribute to the cross-bridging strength [97].

Given the prevailing controversy regarding the existence and mechanism of NF cross-bridging, it is important to note a previous rheological study which was also able to *directly* identify a short critical NF cross-bridging site[5]. The elastic modulus of phos-

[5] Other studies showed that NF phsohporylation increases tail attractive interactions [52, 94]. However,

phorylated NF networks was controlled using free lysine-serine-proline (KSP) synthetic peptides. This demonstrated the involvement of the multiple KSP repeat units, common in the NF-H tail, in tail-mediated NF interactions [38]. Notably, the new electrostatic cross-bridging sites we identified in NF-L (*i.e.* the tip region) are inherently different from the NF the interaction sites reported in the rheological study [38]. While the phosphorylated serine is divalently-charged at biological *p*H levels, all other naturally occurring amino-acid residues are monovalently-charged. Therefore, we find that phosphorylation and divalent monomer charge in general are not perquisites of electrostatic cross-bridging in IDPs and polyampholytes. This considerably increases the frequency and significance of electrostatic-cross bridging in IDPs and polyampholytes in general, which was rarely considered before. Consequently, more attention should be drawn to the role of these weak physical bonds in polyampholyte polymers.

The experimental evidence of electrostatic cross-bridging presented in this thesis (sections 2.1 and 2.4) does not exclude additional cross-bridging mechanisms, such as hydrophobic interactions [34, 98]. In fact, some of our experimental results indicate that non-electrostatic attractive interactions are also implicated in NF cross-bridging. For example, NF-L filaments form a phasse-separated hydrogel at environmental conditions which do not favor electrostatic cross-bridging, including 1 M monovalent NaCl (Fig. 3 in section 2.3). Furthermore, truncation of an NF-L tail segment, which contained two hydrophobic alanine amino-acids considerably expanded the NF-LM network inter-filament spacing (Fig. 1 therein). This suggested that hydrophobic interactions are responsible for attractive forces which give rise to the NF-LM collapsed conformation. Since most experimental efforts thus far focused on proving or negating the role of electrostatic cross-bridges, these results call for specific experimental work, aimed at identifying other cross-bridging mechanisms such as hydrogen-binding and hydrophobic interactions. Notably, these mechanisms were recently shown to affect the tail-mediated interactions and pathology of other intermediate filaments, such as vimentin and desmin (section 2.2 and Refs. [99, 100]).

The significant role of specific short motifs in determining protein properties sets IDPs apart from the charged chains usually considered in classical polymer physics. In other words, a minute modification of an IDP critical site is followed by considerable structural

---

as theoretically demonstrated in Ref. [34], these attraction forces do not prove a direct involvement of phosphate groups in attractive interactions. Instead, the theoretical calculation suggest that NF tail phosphorylation can expose hydrophobic tail amino-acids which induce the observed attraction. Consequently, the authors argue that the cross-bridging reported in these experiments is hydrophobic in nature, not electrostatic. The identification of the cross-bridging sites, achieved by Gou *et. al.* in Ref. [38] cannot be attributed to hydrophobic interactions.

modification, whereas any small change made to a long polymer has a negligible effect. This poses IDP cross-bridging sites as mutation hotspots, whose modification is followed by adverse structural, mechanical and biological consequences. In fact, IDP mutations and modifications are commonly involved in pathological disorders, which is now referred to as "disorder in disorders", or D^2 [1]. The ability to identify, either by experiment or sequence-based analysis, the critical binding-sites found in IDPs could promote the treatment of IDP related diseases. The hansdshake analysis presented and experimentally verified in sections 2.1, 2.3 and 2.4 can help locate critical electrostatic binding-sites.

Persistence length and liquid-crystalline behavior of polymer bottlebrushes

The liquid-crystalline behavior of charged rod-like molecules (section 2.7) as well as charged (sections 2.1, 2.3 and 2.4) and neutral (sections 2.5 and 2.6) bottlebrushes were investigated. Together, these experiments present a puzzling picture, where directional orientation can be either promoted or destroyed by molecular crowding and electrostatic interactions.

For neutral bottlebrush polymers, two key findings are reported. First, using dynamic light scattering and SAXS, we showed that a polymer's aspect ratio decreased due to bottlebrush coating, in contrast to previous theoretical predictions [72]. Second, using SAXS and molecularly detailed calculations, we showed that extensive crowding conditions can reduce the aspect ratio between the backbone's persistence length and the brush height. Taken together, these novel results explain why anisotropic bottlebrush phases are rarely observed (see section 2.6 and Ref. [12]).

The loss of bottlebrush stiffness due to crowding (section 2.6) suggests a possible re-entrant isotropic phase of bottlebrushes (Fig. 4.2). At low free polymer concentrations, the bottlebrushes are isotropic. With increasing free polymer concentrations, bottlebrushes' volume fraction increases as they organize anisotropically. However, a further increase of the free polymer concentration (beyond the overlap concentration described in section 2.6) cancels the osmotic effect and the isotropic phase is recovered. Notably, the loss of stiffening as well as the predicted re-entrant isotropic phase are unique traits of bottlebrush polymers, which are not expected for rod-like particles (section 2.7). An experimental corroboration of this prediction will support the theoretical calculation performed for the neutral bottlebrushes.

The liquid-crystalline behavior of NFs, which are polyampholyte bottlebrushes, requires a more complicated description. This behavior is neither explained by the theoretical model developed for their neutral counterparts nor for the rod-like charged particles.

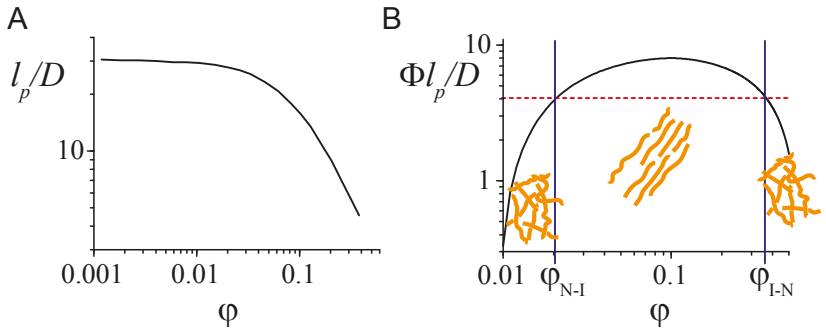

Figure 4.2: Qualitative prediction of re-entrant isotropic phase, based on the detailed calculation appearing in Fig. 10 at section 2.6. (A) The bottlebrush aspect ratio between persistence length (l_p) and width (D) decreases with increasing free polymer volume fraction (φ). According to Onsager (section 1.5), transition to anisotropic phase occurs at $l_k\Phi/D_{eff} \approx 4$, where Φ is the bottlebrush volume fraction and $D \sim D_{eff}$. (B) Consequently, a re-entrant transition is expected at high free polymer concentrations which exceed the overlap concentration (φ_{I-N}).

For example, the charged rod-like viruses organize anisotropically at low ionic strengths and high *p*H, which is explained by an extended Onsager theory [101]. The virus is considered to have a salt-dependent hard-rod equivalent diameter, d_{eff}, which is large at low ionic strength and shrinks towards the hard rod diameter as ionic strength is increased. Its persistence length, however, is always much larger than the virus's length (L in section 1.5) and therefore does not affect the aspect ratio (Eq. 1.9). In contrast, in NFs both the brush height, which should scale with d_{eff}, and persistence length (l_p in section 1.5) vary with the ionic strength. This makes the dependence of their aspect ratio on ionic strength and electrostatic charge unclear[6].

Trying to establish a relation between anisotropy and electrostatics from our experimental results provides an ambiguous picture. For example, NF-H containing networks are isotropic at low salt concentrations, suggesting that electrostatics destabilize the nematic organization. In contrast, enzymatic charge removal in NF-H tail also induces a transition from nematic to isotropic, indicating that charge stabilizes the nematic phase (section 2.4).

These seemingly contradicting trends probably arise from the prominent role of NF cross-bridging in setting the orientational organization. In sections 2.5 and 2.6 we argued that anisotropic organization of bottlebrushes is uncommon. However, NFs phase-

[6] Moreover, the NF brush is softer than the backbone of the virus, and it is therefore uncertain if the extended Onsager model, and d_{eff} in particular, is applicable.

separate from the solution, even without external forces, and form a liquid crystal. The origins of this atypical liquid-crystalline organization can be understood by considering the instances where an isotropic NF organization is observed. These instances include the de-phosphorylated NF-LH networks as well as the truncated NF-L variants and their co-assemblies with NF-M (sections 2.3 and 2.4). In these cases, the NF cross-bridging is debilitated due to dephosphorylation (NF-LH) or due to the removal of critical binding segments (NF-L). It is plausible that the resultant reduction in the attractive forces between the filaments leads to an isotropic transition, similar to the Maier-Saupe theory [102]. There, the attractive orientation-dependent van der Waals attraction between the molecules favors a parallel arrangement of molecules. Consequently, I suggest that the attractive cross-bridging also facilitates the anisotropic transition of NF bottlebrushes, and may explain their atypical nematic organization.

Unfortunately, the relation between NF cross-bridging and anisotropy is made more complex, since cross-bridging not only affects the inter-filament attraction, but also the bottlebrushes' morphology. Namely, increasing cross-bridging can reduce the brush height (and therefore the filament number concentration) and even persistence length [103]. Therefore, the effect of the cross-bridging on the two key factors in Onsager's theory (Eq. 1.9), *i.e.* the aspect ratio $l_{\mathrm{k}}/d_{\mathrm{eff}}$ and volume fraction, is unclear. Elucidating the role of NF cross-bridging requires experiments which will solve the intricate relations between ionic strength, brush height, filament concentration, cross-bridging, and anisotropy in the bottlebrush solution. Such experiments necessitate an exceptionally tight control of many parameters, which is provided by the cross-polarized compatible microfluidic device developed in section 2.7.

The use of microfluidic devices also facilitates the study of NF liquid-crystalline behavior under confinement (*i.e.* the shape of the microfluidic cell). In section 2.7 we showed that the domain size of the nematic phase of *fd*-viruses depends on the confining cell in which it was formed (compare Figs. 2a and 2g therein [104]). Similarly, Hesse *et. al.* self-assembled NFs in nano-channels and formed liquid crystals which were more oriented than those obtained in wider capillaries. The ability to mold the PDMS cell in the microfluidic device can help establish the relation between the anisotropic organization and the geometric confinement. Notably, this relation also makes a biologically relevant problem, since NFs form the supportive skeleton of neurons.

Neuron cells contain multiple regions, distinct by their shape and size (*e.g.* Soma, axon and dendrites). The geometries of these regions change during development to accommodate the evolving needs of the cells [41, 81]. The space-filling NF skeletons which support each of these regions is also specific, and may vary in composition and phospho-

rylation levels. Accordingly, NF alignment is not uniform: the less phosphorylated NF filaments of the Soma appear un-oriented, while the highly phosphorylated NFs of the distal axon appear well-aligned [81].

Understanding the liquid-crystalline behavior of NFs poses a special challenge, as it encompasses most of the problems tackled in this thesis: brush height, cross-bridging and (neutral) bottlebrush anisotropic organization. However, its future investigation can rely on the tools developed in our current research. Theoretically, the molecularly-detailed mean-field model (section 2.6) can be expanded to NFs by combining it with the interaction scheme used in Ref. [34] to study the brush profiles of NFs. Experimentally, the microfluidic device developed in section 2.7 enables, for the first time, to manipulate concentration, ionic strength and to conveniently mold the confining cell's geometry.

Relevance to other biological polymer brush systems

Given the useful properties of NF bottlebrush as structural scaffolds, and their mutable binding and mechanics, it not surprising to find other polymer brush systems in biology. In the following section I will briefly review different protein brush or glycoprotein[7] brush complexes [105].

Notable IDP brushes include the bottlebrush complex formed by microtubules (MTs) decorated with microtubules associated proteins (MAPs), other IF networks, and the FG nucleoporins that form an iris-like gate between the cytoplasm and the nucleus (nuclear pores).

MTs build a filamentous protein network that forms the cytoskeleton by inter-connecting with actin and IF networks (Fig. 1.4). Intrisically disordered MAPs, such as tau protein, non-covalently attach to the smooth MT cylinders to produce a bottlebrush architecture. The grafted tau cross-links adjacent MTs while sterically stabilizing them against bundling [89]. The binding mechanism between two tau proteins attached to opposing MTs is thought to be electrostatic, similar to the mechanism reported here for NFs. Tau proteins also contain multiple phosphrylation sites that control the binding between filaments, as observed in NF-M and NF-H tails. Nonetheless, there are several key differences between the cytoskeletal MTs and NFs. First, MTs persistence length is over 1 mm while NFs persistence length is only few hundreds of nm's long. NF brush height ranges between 15-45 nm, while MTs grafted with tau is less than 2.5 nm. And last, MAPs

[7] Glycoproteins are proteins that contain oligosaccharide chains (glycans) covalently attached to protein side-chains.

are non-covalently attached to MTs, unlike the NF tails which are part of the polypeptide chain. Differences and similarities of IF and MT architectures must be viewed with respect to their roles and interaction in the cytoskeleton.

The roles of tail brushes formed by IFs in general (*i.e.*, not just NFs) were covered in section 2.2. While there are 70 human genes expressing IF proteins, most studies of the disordered tails have so far focused on a handful of keratins, vimentin, four NF and desmin proteins only. In all cases, a critical role of tail mediated binding was reported. For example, desmin tail mutations that appear desminopathy diseases were found to have a detrimental effect on the elasticity of desmin IF networks (see chapter 3 in Ref. [106]). Evidently, more research is required in order to understand this large family of bottlebrush filaments, not the least because of their involvement in disease. The tools developed in this thesis can be naturally be expanded into other IF proteins.

A different binding mechanism and architecture of IDP brushes is found in nuclear pores [30, 107]. Nuclear pores are large protein complexes that cross the nuclear envelope, which is the double membrane surrounding the cell nucleus. Nuclear pores act as gates between the nucleus that contains most of the genetic material and the rest of the cell surrounding it (cytoplasm). A dense brush composed of intrinsically disordered FG-nucleoporin proteins forms an iris-like ring that selectively controls the import and export through the pores. The selectivity is achieved by hydrophobic interactions of the repeating amino acid residues phenylalanine and glycine found on the FG-nucleoporin with themselves, the cargo, and auxiliary signaling proteins. The hydrophobic patches and the resultant binding of FG-nuceloporins are evolutionary conserved, reminiscent of the NF-Ls negatively charged tip we found in Ref. [108] (see Fig. S7). While similar hydrophobic binding patches were identified in the K8 keratin tail [109], the prevalence of hydrophobic interactions on IF tails has yet to be determined.

Three examples of glycoproteins systems are the glycocalyx, the glycomacropeptides surrounding the casein micelles in milk, and aggrecan molecules. The *glycocalyx* is an extracellular layer surrounding many animal cell types and bacteria. It can approximately 150 nm and consists a myriad of carbohydrate-rich molecules, polysaccharides, glycoproteins, and glycolipids[8]. Among its other roles, the glycocalyx mediates the adhesion interactions such cells and protects the plasma membrane from chemical injury [110]. Similar protection is provided by phosphorylated NF tails, which can protect the NF network from proteolytic digestion[9] [111, 112].

[8] A glycolipid consists of an hydrophobic lipid tail and one or more hydrophilic sugar groups linked by a covalent glycosidic bond.

[9] Proteolysis is the digestion (cleavage of the protein chain) by designated proteins, called proteases.

The *glycomacropeptides*[10] are short negatively charged C-terminal ends (≈60 amino acids) of kappa-casein protein, which coat casein micelles in milk. Each casein micelle is a highly porous globular aggregate of approximately 100 nm in diameter. It is thought that interacting glycomacropeptides brushes prevent large micellar aggregation, thus hindering precipitation of the casein micelles and facilitating their digestion. The internal organization of the micelle by the intrinsically disoredered casein proteins is still debated, despite extensive research performed in the past 100 years [113]. The methodology used in this thesis to identify and manipulate electrostatic binding between IDPs could shed a new light on the critical IDP-mediated binding in casein micelles and in the glycocalyx.

Perhaps the most famous glycoprotein brush is formed by the load-bearing aggrecan molecules in the extracellular matrix. Aggrecan is a critical component for cartilage structure and the function of joints, and is also vital for the organization of extracellular spaces between neurons in the brain. An aggrecan molecule is composed of a core protein (250 kDa) that is grafted by 100 negatively charged saccharide chains. The compression mechanism of extracellular aggrecans and cytoplasmic NFs is very similar. In both cases, the highly negatively charged tails produce a repulsive ionic osmotic pressure against external compression. Notably, in NFs the brush consists of the protein C-terminal, whereas the aggregan brush is composed of grafted oligosaccharide chains. Moreover, aggrecan molecules can graft unto hyaluronic acid, which results with the characteristic 'bottlebrush of bottlebrushes' architecture in joints [114].

In summary, despite the many differences in scale, geometry, and basic building blocks, there are clear similarities in the design and roles of the various biological brushes. Consequently, the physical analysis of any system provides valuable model and ideas for their collective investigation. This is especially important given the multiple opens questions regarding nuceloporins interactions and organization, casein-micelle internal structure, cartilage degradation, cellular signaling, and the prevalence of acute diseases accompanied by structural disorders of cytoskeletal proteins.

Future experiments and perspectives

To conclude my thesis, I wish to present additional experiments that, in my opinion, are required to meet the multiple open question and opportunities presented by my thesis.

In sections 2.3 and 2.4 we have identified cross-bridging motifs of NF-L and phosphorylated NF-M. However, identification and future quantification of the binding energies

[10] Also known as caseinomacropeptides.

call for complementary experimental techniques, such as bulk or micro-rheologies of the NF hydrogels. As of today, such experiments successfully identified critical cross-linking motifs in other IF proteins, including desmin and vimentin [106].

In section 2.3, we fitted the compression response of NFs using a modified Alexander-de Gennes brush model. However, at low ionic strengths (below 100 mM) the data are neither adequately explained by the models employed, nor by the simulations and calculations made by our colleagues. Since polyelectrolyte semi-dilute solutions are well understood, the surprisingly large repulsive forces we measure should be re-examined. If the compression response arises from the disordered tails, as we suggest, this considerable excessive repulsion should also appear in a simple solution made of the tails alone (*i.e.*, ungrafted from the filament backbones). This naturally calls for osmotic pressure measurements of semi-dilute tail solutions at various ionic strengths. The concentrations can be measured by the protein absorbance at 280 nm or from the polyelectrolyte peak observed in SAXS measurements[11].

Such experiments may also help clarify the atypical scaling of IDP size with number of amino-acids, reported in Ref. [116]. There, it was found that IDP radius of gyration grows as $R_G = 0.193 N_{aa}^{\nu}$ [nm], where N_{aa} is the number amino acids and $\nu = 0.522$. In contrast, chemically unfolded proteins scaled as $\nu = 0.6$, which is actually closer to the theoretical $nu = 0.588$ obtained for self-avoiding polymers [6, 117]. This discrepancy suggested that IDPs are inherently different from self-avoiding and interacting polymers, which was not so surprising. However, what I find more striking is that IDPs follow a scaling law at all: this suggests that a general IDP model exists, which is yet to be found.

[11] NF-L [87] and NF-H [115] tails can be recombinantly over-expressed and purified.

References

[1] Uversky VN (2011) Intrinsically disordered proteins from A to Z. *Int. J. Biochem. Cell Biol.* 43(8):1090–1103.

[2] Almagor L, Avinery R, Hirsch JA, Beck R (2013) Structural flexibility of CaV1.2 and CaV2.2 I-II proximal linker fragments in solution. *Biophys. J.* 104(11):2392–2400.

[3] Rubinstein M, Colby R (2003) *Polymer Physics*. (Oxford).

[4] Rubinstein M (2010) Polymer physics-The ugly duckling story: Will polymer physics ever become a part of proper physics? *J. Polym. Sci. Part B Polym. Phys.* 48(24):2548–2551.

[5] De Gennes PG (1979) *Scaling concepts in polymer physics*. (Cornell university press).

[6] Grosberg A, Khokhlov A (1994) *Statistical physics of macromolecules*. (AIP, New York).

[7] Rubinstein M, Papoian GA (2012) Polyelectrolytes in biology and soft matter. *Soft Matter* 8(36):9265.

[8] Dobrynin AV, Colby RH, Rubinstein M (2004) Polyampholytes. *J. Polym. Sci. Part B Polym. Phys.* 42(19):3513–3538.

[9] Dobrynin AV, Rubinstein M (2005) Theory of polyelectrolytes in solutions and at surfaces. *Prog. Polym. Sci.* 30(11):1049–1118.

[10] Bracha D, Karzbrun E, Shemer G, Pincus PA, Bar-Ziv RH (2013) Entropy-driven collective interactions in DNA brushes on a biochip. *Proc. Natl. Acad. Sci.* 110(12):4534–4538.

[11] Azzaroni O (2012) Polymer brushes here, there, and everywhere: Recent advances in their practical applications and emerging opportunities in multiple research fields. *Journal of Polymer Science Part A: Polymer Chemistry* 50(16):3225–3258.

[12] Raviv U et al. (2003) Lubrication by charged polymers. *Nature* 425(6954):163–165.

[13] Borisov OV, Zhulina EB, Birshtein TM (1994) Diagram of the States of a Grafted Polyelectrolyte Layer. *Macromolecules* 27(17):4795–4803.

[14] Zhulina EB, Birshtein TM, Borisov OV (1995) Theory of Ionizable Polymer Brushes. *Macromolecules* 28(5):1491–1499.

[15] Armstrong G (2012) DNA replication: High fidelity. *Nature Chemistry* 4(8):592–593.

[16] Saleh OA, McIntosh DB, Pincus P, Ribeck N (2009) Nonlinear Low-Force Elasticity of Single-Stranded DNA Molecules. *Phys. Rev. Lett.* 102(6):068301.

[17] de Gennes P (1980) Conformations of polymers attached to an interface. *Macromolecules* 13(5):1069–1075.

[18] Alexander S (1977) Adsorption of chain molecules with a polar head a scaling description. *J. Phys.* 38(8):983–987.

[19] Daoud M, Cotton J (1982) Star shaped polymers: a model for the conformation and its concentration dependence. *Journal de Physique* 43(3):531–538.

[20] Milner ST (1991) Polymer brushes. *Science* 251(4996):905–914.

[21] Zhulina E, Leermakers F (2007) Effect of the Ionic Strength and pH on the Equilibrium Structure of a Neurofilament Brush. *Biophys. J.* 93(5):1452–1463.

[22] Leermakers FAM, Zhulina EB (2010) How the projection domains of NF-L and α-internexin determine the conformations of NF-M and NF-H in neurofilaments. *Eur. Biophys. J.* 39(9):1323–1334.

[23] Skvortsov AM, Klushin LI, Gorbunov AA (1997) Long and short chains in a polymeric brush: a conformational transition. *Macromolecules* 30(6):1818–1827.

[24] Kornreich M et al. (2015) Composite bottlebrush mechanics: α-internexin fine-tunes neurofilament network properties. *Soft Matter* 11(29):5839–5849.

[25] Hansen PL, Cohen JA, Podgornik R, Parsegian VA (2003) Osmotic Properties of Poly(Ethylene Glycols): Quantitative Features of Brush and Bulk Scaling Laws. *Biophysical Journal* 84(1):350–355.

[26] Dobrynin AV, Colby RH, Rubinstein M (1995) Scaling Theory of Polyelectrolyte Solutions. *Macromolecules* 28(6):1859–1871.

[27] Pincus P (1991) Colloid Stabilization with Grafted Polyelectrolytes. *Macromolecules* 24(10):2912–2919.

[28] Rogers WB, Crocker JC (2011) Direct measurements of DNA-mediated colloidal interactions and their quantitative modeling. *Proc. Natl. Acad. Sci.* 108(38):15687–15692.

[29] Eiser E, Klein J, Witten TA, Fetters LJ (1999) Shear of Telechelic Brushes. *Phys. Rev. Lett.* 82(25):5076–5079.

[30] Uversky VN (2013) A decade and a half of protein intrinsic disorder: Biology still waits for physics. *Protein Science* 22(6):693–724.

[31] Hirokawa N, Glicksman MA, Willard MB (1984) Organization of mammalian neurofilament polypeptides within the neuronal cytoskeleton. *J. Cell Biol.* 98(4):1523–36.

[32] Hisanaga S, Hirokawa N (1988) Structure of the peripheral domains of neurofilaments revealed by low angle rotary shadowing. *J. Mol. Biol.* 202(2):297–305.

[33] Janmey PA, Leterrier JF, Herrmann H (2003) Assembly and structure of neurofilaments. *Curr. Opin. Colloid Interface Sci.* 8(1):40–47.

[34] Leermakers FAM, Zhulina EB (2008) Self-consistent field modeling of the neurofilament network. *Biophys. Rev. Lett.* 3(04):459–489.

[35] Kumar S, Yin X, Trapp BD, Hoh JH, Paulaitis ME (2002) Relating interactions between neurofilaments to the structure of axonal neurofilament distributions through polymer brush models. *Biophys. J.* 82(5):2360–2372.

[36] Stevens MJ, Hoh JH (2011) Interactions between planar grafted neurofilament sidearms. *J. Phys. Chem. B* 115(23):7541–7549.

[37] Stevenson W, Chang R, Gebremichael Y (2011) Phosphorylation-mediated conformational changes in the mouse neurofilament architecture: insight from a neurofilament brush model. *J. Mol. Biol.* 405(4):1101–18.

[38] Gou JP, Gotow T, Janmey PA, Leterrier JF (1998) Regulation of neurofilament interactions in vitro by natural and synthetic polypeptides sharing Lys-Ser-Pro sequences with the heavy neurofilament subunit NF-H: Neurofilament crossbridging by antiparallel sidearm overlapping. *Med. Biol. Eng. Comput.* 36(3):371–387.

[39] Sinha S (2004) Regulation of Intermediate Filament Gene Expression in *Intermed. Filam. Cytoskelet.*, eds. M. Bishr Omary, in Cell Biology PACBTM. (Academic Press) Vol. Volume 78, pp. 267–296.

[40] Omary MB (2004) *Intermediate Filament Cytoskeleton, Volume 78.* (Gulf Professional Publishing), p. 886.

[41] Laser Azogui A, Kornreich M, Malka-Gibor E, Beck R (2014) Neurofilament assembly and function during neuronal development. *Curr. Opin. Cell Biol.* 32(Cell architecture):92–101.

[42] Alberts B et al. (2002) *Molecular biology of the cell.* (Garland).

[43] Kyte J, Doolittle RF (1982) A simple method for displaying the hydropathic character of a protein. *J. Mol. Biol.* 157(1):105–132.

[44] Liu Q et al. (2011) Neurofilamentopathy in neurodegenerative diseases. *The open neurology journal* 5:58–62.

[45] Rao MV et al. (2003) The neurofilament middle molecular mass subunit carboxyl-terminal tail domains is essential for the radial growth and cytoskeletal architecture of axons but not for regulating neurofilament transport rate. *J. Cell Biol.* 163(5):1021–31.

[46] Mukhopadhyay R, Kumar S, Hoh JH (2004) Molecular mechanisms for organizing the neuronal cytoskeleton. *BioEssays* 26(9):1017–1025.

[47] Price RL, Paggi P, Lasek RJ, Katz MJ (1988) Neurofilaments are spaced randomly in the radial dimension of axons. *Journal of Neurocytology* 17(1):55–62.

[48] Fuchs E (1998) A Structural Scaffolding of Intermediate Filaments in Health and Disease. *Science (80-.).* 279(5350):514–519.

[49] Stevens MJ, Hoh JH (2010) Conformational dynamics of neurofilament side-arms. *J. Phys. Chem. B* 114(27):8879–8886.

[50] Jayanthi L, Stevenson W, Kwak Y, Chang R, Gebremichael Y (2013) Conformational properties of interacting neurofilaments: Monte Carlo simulations of cylindrically grafted apposing neurofilament brushes. *J. Biol. Phys.* 39(3):343–362.

[51] Brown HG, Hoh JH (1997) Entropic exclusion by neurofilament sidearms: A mechanism for maintaining interfilament spacing. *Biochemistry* 36(49):15035–15040.

[52] Aranda-Espinoza H, Carl P, Leterrier JF, Janmey P, Discher DE (2002) Domain unfolding in neurofilament sidearms: effects of phosphorylation and ATP. *FEBS Lett.* 531(3):397–401.

[53] Beck R, Deek J, Jones JB, Safinya CR (2010) Gel-expanded to gel-condensed transition in neurofilament networks revealed by direct force measurements. *Nat. Mater.* 9(1):40–46.

[54] Jeong S, Zhou X, Zhulina EB, Jho Y (2016) Monte Carlo Simulation of the Neurofilament Brush. *Israel Journal of Chemistry* 56(8):599–606.

[55] Zhulina EB, Leermakers FAM (2009) On the polyelectrolyte brush model of neurofilaments. *Soft Matter* 5(15):2836.

[56] Yuan A, Rao MV, Veeranna, Nixon RA (2012) Neurofilaments at a glance. *J. Cell Sci.* 125(Pt 14):3257–63.

[57] Smith DH, Wolf JA, Lusardi TA, Lee VMY, Meaney DF (1999) High Tolerance and Delayed Elastic Response of Cultured Axons to Dynamic Stretch Injury. *The Journal of Neuroscience* 19(11):4263 LP – 4269.

[58] McHale MK, Hall GF, Cohen MJ (1995) Early cytoskeletal changes following injury of giant spinal axons in the lamprey. *The Journal of Comparative Neurology* 353(1):25–37.

[59] Hodgkin AL, Huxley AF (1952) A quantitative description of membrane current and its application to conduction and excitation in nerve. *The Journal of Physiology* 117(4):500–544.

[60] Garcia ML et al. (2003) NF-M is an essential target for the myelin-directed "outside-in" signaling cascade that mediates radial axonal growth. *J. Cell Biol.* 163(5):1011–1020.

[61] Rao MV et al. (2002) Gene replacement in mice reveals that the heavily phosphorylated tail of neurofilament heavy subunit does not affect axonal caliber or the transit of cargoes in slow axonal transport. *J. Cell Biol.* 158(4):681–693.

[62] Križ J, Zhu Q, Julien JP, Padjen AL (2000) Electrophysiological properties of axons in mice lacking neurofilament subunit genes: disparity between conduction velocity and axon diameter in absence of NF-H. *Brain Res.* 885(1):32–44.

[63] Shen H, Barry DM, Garcia ML (2010) Distal to proximal development of peripheral nerves requires the expression of neurofilament heavy. *Neuroscience* 170(1):16–21.

[64] Garcia ML et al. (2009) Phosphorylation of highly conserved neurofilament medium KSP repeats is not required for myelin-dependent radial axonal growth. *J. Neurosci.* 29(5):1277–84.

[65] Nguyen MD, Larivière RC, Julien JP (2001) Deregulation of Cdk5 in a Mouse Model of ALS. *Neuron* 30(1):135–148.

[66] Lobsiger CS, Garcia ML, Ward CM, Cleveland DW (2005) Altered axonal architecture by removal of the heavily phosphorylated neurofilament tail domains strongly slows superoxide dismutase 1 mutant-mediated ALS. *Proceedings of the National Academy of Sciences* 102(29):10351–10356.

[67] Rao MV et al. (2011) The Myosin Va Head Domain Binds to the Neurofilament-L Rod and Modulates Endoplasmic Reticulum (ER) Content and Distribution within Axons. *PLoS ONE* 6(2):e17087.

[68] Barry DM et al. (2012) Expansion of Neurofilament Medium C Terminus Increases Axonal Diameter Independent of Increases in Conduction Velocity or Myelin Thickness. *Journal of Neuroscience* 32(18):6209–6219.

[69] Yuan A, Nixon RA (2016) Specialized roles of neurofilament proteins in synapses: Relevance to neuropsychiatric disorders. *Brain Research Bulletin* 126:334–346.

[70] de Gennes PG, Prost J (1995) *The Physics of Liquid Crystals (International Series of Monographs on Physics)*. (Oxford University Press, USA).

[71] Onsager L (1949) The effects of shape on the interaction of colloidal particles. *Ann. N. Y. Acad. Sci.* 51(4):627–659.

[72] Fredrickson GH (1993) Surfactant-induced lyotropic behavior of flexible polymer solutions. *Macromolecules* 26(11):2825–2831.

[73] Feuz L, Leermakers FaM, Textor M, Borisov O (2005) Bending Rigidity and Induced Persistence Length of Molecular Bottle Brushes: A Self-Consistent-Field Theory. *Macromolecules* 38(21):8891–8901.

[74] Malka-Gibor E et al. (2016) Phosphorylation-induced mechanical regulation of intrinsically disordered neurofilament protein assemblies. *In preparation*.

[75] Storm IM et al. (2015) Liquid Crystals of Self-Assembled DNA Bottlebrushes. *The Journal of Physical Chemistry B* 119(10):4084–4092.

[76] Selinger JV, Bruinsma RF (1991) Hexagonal and nematic phases of chains .1. Correlation-functions. *Phys. Rev. A* 43(6):2922–2931.

[77] Jones JB, Safinya CR (2008) Interplay between Liquid Crystalline and Isotropic Gels in Self-Assembled Neurofilament Networks. *Biophys. J.* 95(2):823–835.

[78] Deek J, Chung PJ, Kayser J, Bausch AR, Safinya CR (2013) Neurofilament sidearms modulate parallel and crossed-filament orientations inducing nematic to isotropic and re-entrant birefringent hydrogels. *Nat. Commun.* 4:2224.

[79] Hesse HC et al. (2008) Direct imaging of aligned neurofilament networks assembled using in situ dialysis in microchannels. *Langmuir* 24(16):8397–401.

[80] Barry DM et al. (2010) Variation of the neurofilament medium KSP repeat subdomain across mammalian species: implications for altering axonal structure. *J. Exp. Biol.* 213(1):128–136.

[81] Safinya CR, Deek J, Beck R, Jones JB, Li Y (2015) Assembly of Biological Nanostructures: Isotropic and Liquid Crystalline Phases of Neurofilament Hydrogels. *Annu. Rev. Condens. Matter Phys.* 6(1):113–136.

[82] Monsma PC, Li Y, Fenn JD, Jung P, Brown A (2014) Local regulation of neurofilament transport by myelinating cells. *J. Neurosci.* 34(8):2979–88.

[83] Lieleg O, Claessens MMAE, Luan Y, Bausch AR (2008) Transient Binding and Dissipation in Cross-Linked Actin Networks. *Phys. Rev. Lett.* 101(10):108101.

[84] Carden MJ, Trojanowski JQ, Schlaepfer WW, Lee VM (1987) Two-stage expression of neurofilament polypeptides during rat neurogenesis with early establishment of adult phosphorylation patterns. *J. Neurosci.* 7(11):3489–504.

[85] Deek J (2012) Ph.D. thesis (University of California, Santa Barbara).

[86] Das B, Guo X, Ballauff M (2002) The osmotic coefficient of spherical polyelectrolyte brushes in aqueous salt-free solution in *Molecular Organisation on Interfaces*. (Springer Berlin Heidelberg, Berlin, Heidelberg), pp. 34–38.

[87] Pregent S et al. (2015) Probing the Interactions of Intrinsically Disordered Proteins Using Nanoparticle Tags. *Nano Lett.* 15(5):3080–3087.

[88] Harpaz Y, Gerstein M, Chothia C (1994) Volume changes on protein folding. *Structure* 2(7):641–649.

[89] Chung PJ et al. (2015) Direct force measurements reveal that protein Tau confers short-range attractions and isoform-dependent steric stabilization to microtubules. *Proc. Natl. Acad. Sci.* 112(47):E6416–E6425.

[90] Chung PJ et al. (2016) Tau mediates microtubule bundle architectures mimicking fascicles of microtubules found in the axon initial segment. *Nature Communications* 7:12278.

[91] Borisov OV, Zhulina EB, Leermakers FAM, Ballauff M, M??ller AHE (2011) Conformations and solution properties of star-branched polyelectrolytes. *Adv. Polym. Sci.* 241(1):1–55.

[92] Zhulina EB, Birshtein TM, Borisov OV (2006) Curved polymer and polyelectrolyte brushes beyond the Daoud-Cotton model. *Eur. Phys. J. E. Soft Matter* 20(3):243–256.

[93] Hirokawa N (1982) Cross-linker system between neurofilaments, microtubules and membranous organelles in frog axons revealed by the quick-freeze, deep-etching method. *The Journal of Cell Biology* 94(1):129–142.

[94] Eyer J, Leterrier JF (1988) Influence of the phosphorylation state of neurofilament proteins on the interactions between purified filaments in vitro. *Biochem. J.* 252(3):655–660.

[95] Yabe JT, Jung C, Chan WK, Shea TB (2000) Phospho-dependent association of neurofilament proteins with kinesin in situ. *Cell Motil. Cytoskeleton* 45(4):249–62.

[96] Lee S, Sunil N, Shea TB (2011) C-terminal neurofilament phosphorylation fosters neurofilament-neurofilament associations that compete with axonal transport. *Cytoskeleton (Hoboken).* 68(1):8–17.

[97] Kumar S, Nussinov R (1999) Salt bridge stability in monomeric proteins11Edited by J. M. Thornton. *Journal of Molecular Biology* 293(5):1241–1255.

[98] Zhulina EB, Leermakers FAM (2010) The Polymer Brush Model of Neurofilament Projections: Effect of Protein Composition. *Biophys. J.* 98(3):462–469.

[99] Maddison P et al. (2012) Clinical and Myopathological Characteristics of Desminopathy Caused by a Mutation in Desmin Tail Domain. *Eur. Neurol.* 68(5):279–286.

[100] Bär H et al. (2007) Conspicuous involvement of desmin tail mutations in diverse cardiac and skeletal myopathies. *Hum. Mutat.* 28(4):374–386.

[101] Dogic Z, Purdy KR, Grelet E, Adams M, Fraden S (2004) Isotropic-nematic phase transition in suspensions of filamentous virus and the neutral polymer Dextran. *Phys. Rev. E. Stat. Nonlin. Soft Matter Phys.* 69(5 Pt 1):051702.

[102] Luckhurst GR, Zannoni C (1977) Why is the MaierSaupe theory of nematic liquid crystals so successful? *Nature* 267(5610):412–414.

[103] Beck R et al. (2010) Unconventional salt trend from soft to stiff in single neurofilament biopolymers. *Langmuir* 26(24):18595–18599.

[104] Kornreich M, Heymann M, Fraden S, Beck R (2014) Cross polarization compatible dialysis chip. *Lab Chip* 14(19):3700–4.

[105] Zhulina E (2008) Polymer brushes. *Bulletin of the American Physical Society* 53.

[106] Kornreich M, Avinery R, Malka-Gibor E, Laser-Azogui A, Beck R (2015) Order and disorder in intermediate filament proteins. *FEBS Lett.* 589(19):2464–2476.

[107] Wente SR, Rout MP (2010) The Nuclear Pore Complex and Nuclear Transport. *Cold Spring Harbor Perspectives in Biology* 2(10):a000562–a000562.

[108] Kornreich M, Malka-Gibor E, Zuker B, Laser-Azogui A, Beck R (2016) Neurofilaments Function as Shock Absorbers: Compression Response Arising from Disordered Proteins. *Physical Review Letters* 117(14):148101.

[109] Pawelzyk P, Mücke N, Herrmann H, Willenbacher N (2014) Attractive interactions among intermediate filaments determine network mechanics in vitro. *PLoS One* 9(4):e93194.

[110] Roseman S (2001) Reflections on Glycobiology. *Journal of Biological Chemistry* 276(45):41527–41542.

[111] Pant HC (1988) Dephosphorylation of neurofilament proteins enhances their susceptibility to degradation by calpain. *Biochem. J.* 256(2):665–8.

[112] Goldstein ME, Sternberger NH, Sternberger LA (1987) Phosphorylation protects neurofilaments against proteolysis. *J. Neuroimmunol.* 14(2):149–60.

[113] de Kruif CG, Huppertz T, Urban VS, Petukhov AV (2012) Casein micelles and their internal structure. *Advances in Colloid and Interface Science* 171-172:36–52.

[114] Kiani C, Chen L, Wu YJ, Yee AJ, Yang BB (2002) Structure and function of aggrecan. *Cell Research* 12(1):19–32.

[115] Srinivasan N, Bhagawati M, Ananthanarayanan B, Kumar S (2014) Stimuli-sensitive intrinsically disordered protein brushes. *Nat. Commun.* 5:5145.

[116] Bernadó P, Svergun DI (2012) Structural analysis of intrinsically disordered proteins by small-angle X-ray scattering. *Mol. BioSyst.* 8(1):151–167.

[117] Kohn JE et al. (2004) Random-coil behavior and the dimensions of chemically unfolded proteins. *Proc. Natl. Acad. Sci. U. S. A.* 101(34):12491–12496.

A Appendix: protocols

A.1 Native protein purification protocol

A.2 Recombinant protein purification and expression

A.3 Negative staining of neurofialments for transmission electron microscopy

A.4 Sample preparation for atomic force microscopy

A.5 Protein concentration determination by mini-Bradford assay

A.6 Neurofilament self-assembly protocol

סדר ואי-סדר בחלבוני שלד התא של מערכת העצבים

חיבור לשם קבלת התואר

"דוקטור לפילוסופיה"

ע"י

מיכה קורנרייך

תחת הנחייתו של

פרופ' רועי בק

הוגש לסנאט של אוניברסיטת תל-אביב

נובמבר 2016

תקציר

במשך שנים שררה תמימות דעים לגבי הקשר הישיר בין המבנה התלת-מימדי של חלבונים לבין תפקודם הביולוגי. עם זאת, בעשרים שנים האחרונות התברר כי בערך 50% מהחלבונים האנושיים מכילים אזורים נרחבים שאינם מסודרים מבחינה מרחבית, והם מכונים חלבונים לא מסודרים אינהרנטית (Intrinsically disordered proteins, IDPs). בהמשך התגלה כי לאזורים אלו תפקידים ביולוגיים קריטיים, בניגוד לדעה המקובלת. מכיוון שהקונפורמציות של חלבונים אלו בתנאים פיזיולוגיים מזכירות פולימר גאוסייני, חקירתם של החלבונים מסתייעת באופן טבעי בכלים תיאורטיים וניסויים הלקוחים מפיזיקת הפולימרים וממכניקה סטטיסטית.

אי לזאת, חקר ה- IDPs מצוי בתווך שבין פיזיקה וביולוגיה. מחד גיסא, המורכבות והשונות של IDPs מציגות הזדמנויות ניסיוניות חדשות לפיזיקאים המתמודדים עם שאלות פתוחות בפיזיקת פולימרים. ומאידך גיסא, שימוש בכלים פיזיקליים במחקר IDPs מעודד תובנות חדשות לגבי התפקודים הביולוגיים של חלבונים אלו.

בתזה זו אני חוקר באופן ניסיוני את תגובת הדחיסה ואפיון מצב הנוזל הגבישי של ביו-פולימרים מורכבים, הכוללים את חלבוני שלד התא הנוירונים (neurofilaments, NFs); וקומפלקסים מלאכותיים בצורת מברשת ניקוי בקבוקים, העשויים חומצה דאוקסיריבונוקלאית וחלבון. בשיתוף עם עמיתינו, אני משתמשים בפיזור רנטגן בזוויות קטנות, פיזור אור דינאמי, וכן מיקרוסקופיה אופטית, אלקטרונית וכוח-אטומית כדי למדוד את המבנים והאינטראקציות הפולימריים. אנו נוקטים באנליזה בגישה פיזיקלית, במטרה לחשוף את המנגנונים המולקולריים שבסיס ההתארגנות המבנית של IDPs.

תגובת הדחיסה של התקריש המימי (hydrogel) של NFs נמדד בתנאי סביבה שונים. חלבונים אלו הם IDPs היוצרים פילמנטים מוארכים בקוטר 10 ננומטר, שתצורתם כשל מברשות ניקוי-בקבוקים. הפילמנטים מתעבים לכדי תקריש מימי בריכוזים גבוהים. תפקידם המרכזי הוא לספק תמיכה מכנית לתאים באמצעות אינטראקציות שבין החלקים הבלתי מסודרים המזדקרים מהפילמנטים לעבר התמיסה. תחת תנאים כמו-פיזיולוגיים אנו מראים כי הכוחות הסטריים והאלקטרוסטטיים הדוחים, שאחראיים להתנגדות התקריש לדחיסה, הינם שקולים. בהתאם, אנו מדגימים כיצד תגובת הדחיסה של IDPs ניתנת לשליטה וכוונון יעילים באמצעות מניפולציות ביולוגיות של המטען החשמלי על גבי החלבון. תחת דחיסה משמעותית, התנהגות החלבונים (הטעונים בעיקר במטען שלילי) ניתנת לקירוב מוצלח ע"י מודלים המתאימים לפולימרים בעלי מטען שלילי אחיד. הגמישות של החלקים הלא מסודרים מאפשרת לתקריש ה-NFs להידחס בשיעור של פי 20 מבלי לקרוס, מה שעשוי להסביר מדוע IDPs הינם מרכיב חיוני בשלדים החלבוניים התומכים של תאים.

המטען הלא אחיד של חלבוני ה-NF מתבטא כאשר מידת הדחיסה פחותה יותר, כפי שאנו מגלים ניסיונית בעזרת שינויים גנטיים והתערבות אנזימטית. בדחיסה זו, אנו מוצאים כי גשרים אלקטרוסטטים בין חלקי חלבונים הטעונים במטענים הפוכים אחראיים לגודל התקריש ולהתארגנות הנוזלית-גבישית שלו. ההשפעות דומות של אינטרקציות גשר על ההתארגנות הנוזלית גבישית של פולימרים כמעט ולא נחקרו בעבר, ועשויות להסביר מדוע NFs מתארגנים כגביש נוזלי על אף שהדבר אינו אופייני לפולימרים אחרים מתצורת מברשת ניקוי-בקבוקים.

היכולת לשנות את הגודל, הכיווניות והתגובה המכנית של תקרישי NF בעזרת שינויים לאזורים הלא מסודרים, מדגימה את התפקיד הקריטי של רצף ה- IDPs. משמעו שאי-סדר חלבוני אינו זהה לאקראיות. למעשה, תוצאותינו מראות כי הרצף המסוים, וביחוד המטען החשמלי הנלווה, משנים מאד.